University of Alberta
Department of Civil Engineering

Structural Engineering Report No. 13

Experiments on Wide-Flange Beams Under Moment Gradient

by

R. J. Smith

and

P. F. Adams

May, 1968

EXPERIMENTS ON WIDE-FLANGE BEAMS

UNDER MOMENT GRADIENT

by

R. J. Smith
P. F. Adams

May, 1968

Department of Civil Engineering
University of Alberta
Edmonton, Canada

ABSTRACT

This investigation attempts to define the effect of moment gradient on the rotation capacity of a structural steel member, and to separate the influence of moment gradient from that of the unbraced slenderness ratio.

The results of twelve tests on rolled steel wide-flange beams are reported. The tests were performed on simply-supported beams of CSA G40.12 steel, subjected to a concentrated load at midspan. The flange plate geometry and the laterally unbraced slenderness ratio were varied, while the web plate geometry was held constant. All tests were continued until substantial unloading had occurred due to instability.

The results of the present tests provide sufficient information on which to base a specific design recommendation for the limiting flange slenderness ratio for compact sections used in structures designed by the allowable stress method.

The plastic hinge rotations delivered by the test specimens are compared to the maximum practical requirements for plastically designed continuous beams. For short beams, the requirements can be easily met, but for longer beams, the requirements appear to be excessive. An analytical study is proposed to obtain a closer estimate of the required hinge rotation. This proposed analysis, along with available test results, would allow firm conclusions to be drawn regarding the plastic design of continuous beams.

TABLE OF CONTENTS

CHAPTER I

INTRODUCTION

The plastic design method defines the limit of usefulness of a structure as its maximum load carrying capacity. Plastic design makes conscious use of the complete stress-strain relationship for structural steel. This enables a structure to redistribute internal moments once yielding occurs and results in a load carrying capacity above that predicted by limiting the nominal strains in the material to those within the elastic range.

FIG. 1.1 represents (to an expanded horizontal scale) the idealized initial portion of a stress-strain (σ-ε) curve for structural steel in either tension or compression [1]. For strains below the yield strain, ε_y, the material is elastic, with the slope of the stress-strain curve defined as the elastic modulus, E. For strains greater than ε_y, the stress remains constant at the yield stress, σ_y, and the material deforms up to a strain of ε_{st}, the strain at the onset of strain-hardening. Strains greater than ε_{st} can only take place with an increase in stress. The initial slope of the curve in this range is E_{st}, the strain-hardening modulus.

The "simple plastic" theory assumes that the material in a member cross-section subjected to flexure remains elastic until the "plastic moment", M_p, is reached. At this stage, a stress of $\pm \sigma_y$ is present in all elements of the cross-section. Once the plastic

moment has been reached, the member is able to rotate indefinitely at this constant moment value. In other words, a "plastic hinge" has developed. Thus a redundant structure will develop plastic hinges and will redistribute the increased bending moments produced by further loading until sufficient sections have yielded to produce an unstable linkage or "mechanism".

The behavior assumed in the simple plastic theory neglects the additional moment capacity due to the effects of strain-hardening, however, it also ignores the possibility of instability occurring before the collapse load has been reached. Certain factors, such as local or lateral buckling, limit the actual rotation capacity of a section. Consequently, the ability to deform inelastically at the plastic moment is a function of the loading condition, the adequacy of the bracing system and the material and geometric properties of the member.

FIG. 1.2 plots the maximum moment (under the load), M, non-dimensionalized as M/M_p (where M_p is the plastic moment capacity of the cross-section) versus the relative rotation of the two ends, θ, non-dimensionalized as θ/θ_p (where θ_p is the rotation corresponding to the attainment of M_p assuming ideally elastic behavior). The curves are plotted for a simply supported beam of length, $2L$, subjected to the concentrated load, P, as shown in the inset. The behavior assumed in the simple plastic theory is represented by the dashed lines. The actual behavior, represented by the solid curves, departs from the idealized M-θ curve at first yielding. For a "short" beam the drop-off in moment capacity is a result of local buckling within the yielded portion of the compression flange. The local buckling condition is

related to the flange slenderness ratio (b/t) and possibly to the moment gradient [2]. For specimens of intermediate length unloading is precipitated by lateral deformations of the unbraced span. These deformations produce strains which assist the local flange buckling. As indicated by FIG. 1.2, in both the above cases, M_p is reached and exceeded due to strain-hardening of the material. In other cases, unloading may occur before the attainment of the plastic moment. This behavior is representative of "long" beams in which unloading is precipitated by the large lateral deformations of the unbraced span.

The three plots of FIG. 1.2 represent the behavior of beams subjected to a moment gradient. The behavior typical of short beams would appear to provide adequate rotation capacity (inelastic rotation with $M \geq M_p$) for use in plastically designed structures while that for long beams would not. For beams of intermediate length, the adequacy of the delivered rotation capacity would depend on the inelastic rotation required to form a mechanism in the structure.

Beams subjected to moment gradient have been the subject of both analytical [3,4] and experimental [2,5,6] investigations. However, the results to date have not defined the effects of unbraced length and moment gradient on the hinge capacity. The present investigation attempts to define the effect of moment gradient on the rotation capacity and to separate the influence of moment gradient from that of the unbraced slenderness ratio. In addition, an attempt will be made to differentiate between failure triggered by local buckling and failure which results primarily from large lateral-torsional deformations.

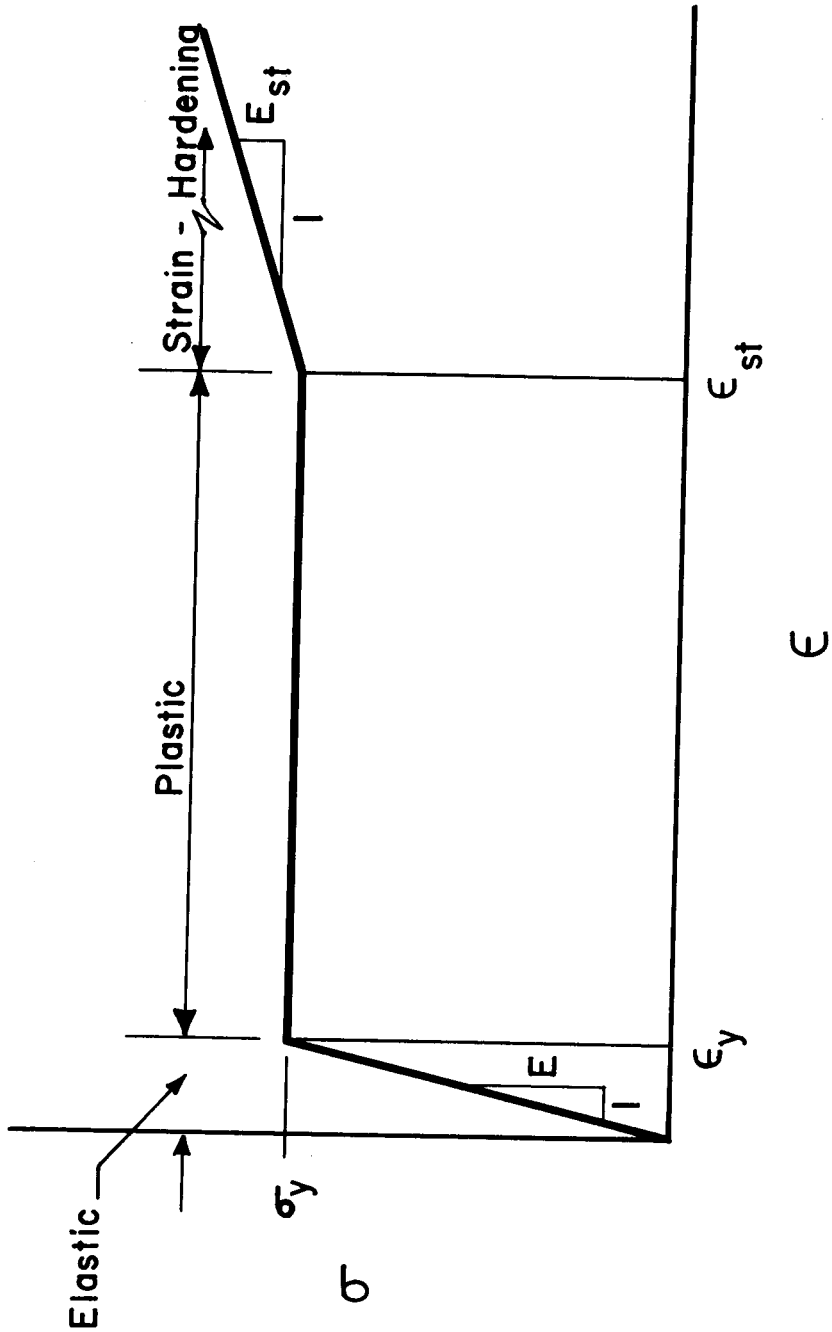

FIGURE 1.1 STRESS-STRAIN RELATIONSHIP

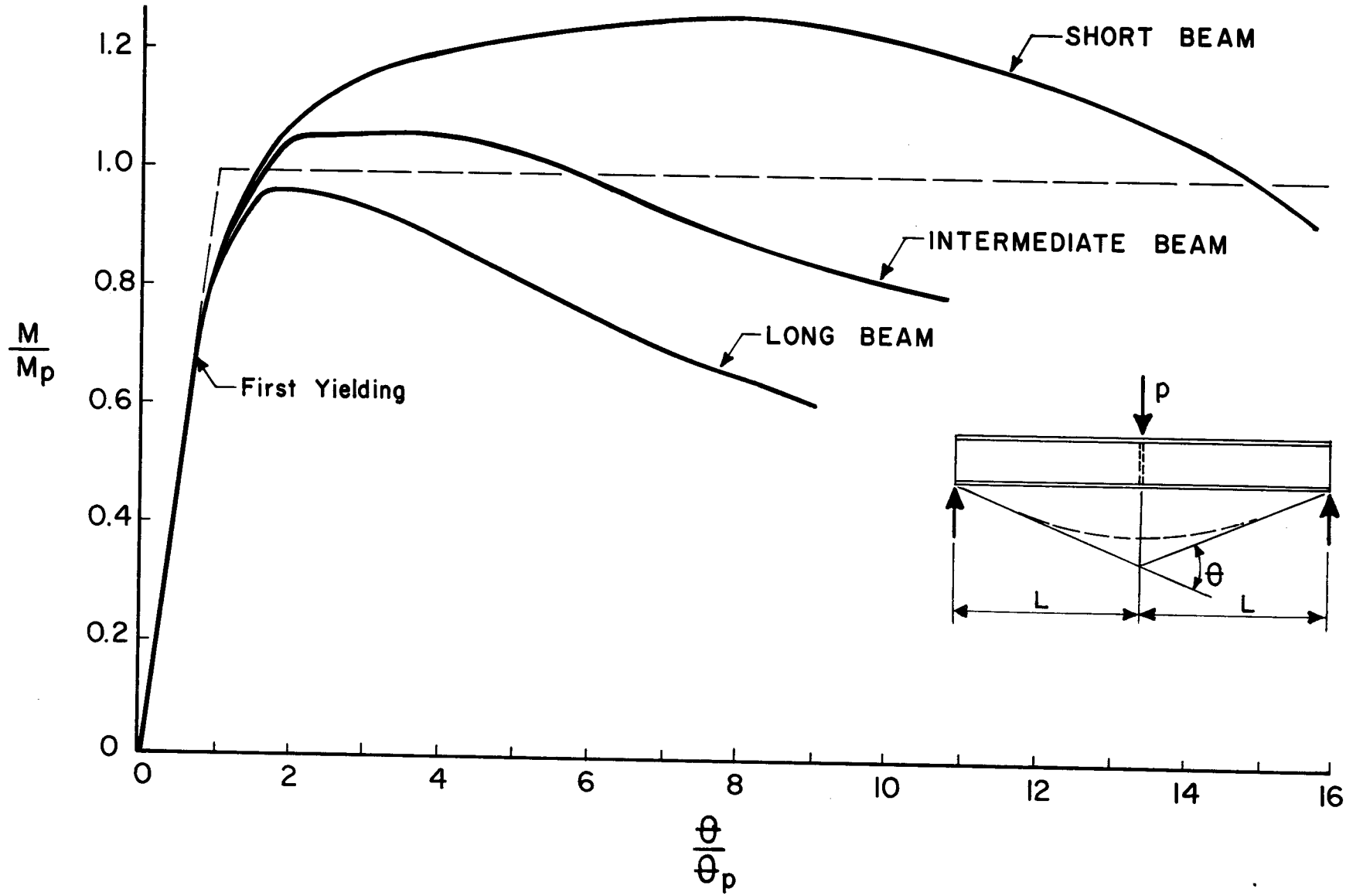

FIGURE 1.2 MOMENT-ROTATION RELATIONSHIPS

CHAPTER II

PREVIOUS INVESTIGATIONS

In order for a steel structure to attain the load predicted by the simple plastic theory, the members must be proportioned so that local or lateral buckling will not prematurely terminate the rotation capacity of the hinging sections.

Lay and Galambos have reported the results of a study of the inelastic behavior of wide-flange beams under moment gradient [3]. The loading condition is illustrated by FIG. 2.1. The applied load, P, is sufficient to produce a midspan moment, $M_o = PL/2$, above the plastic moment, M_p. The yielded length, over which the moment exceeds M_p, is represented by $2\tau L$ in FIG. 2.1(b). The curvature diagram corresponding to this moment distribution is as shown in FIG. 2.1(c). $\phi_p = M_p/EI$ is the curvature corresponding to the attainment of M_p, assuming ideally elastic behavior. The plastic hinge rotation may be approximated by the cross-hatched area in FIG. 2.1(c) [3].

This study indicated that local rather than lateral buckling will initiate unloading of the member for values of λ below approximately 0.7. The slenderness factor, λ, is defined as

$$\lambda = \frac{L}{r_y}\sqrt{\frac{\varepsilon_y}{\pi}} \qquad (2.1)$$

Lay has treated flange local buckling by considering the torsional buckling of the flange [7]. The model used has been described in a previous report and considers the restraining action of the web [2]. In order for a local buckle to form at a minimum stress, the length of flange, τL, which is fully yielded, must equal one full wavelength of the buckled plate. This length is referred to as the optimum yielded length, ℓ_{opt}, given by:

$$\ell_{opt} = 1.42 \frac{bt}{w} \left(\frac{A_w}{A_f} \right)^{1/4} \tag{2.2}$$

In Equation 2.2, b and t are the flange width and thickness respectively while w is the web thickness. A_w represents the area of the web and A_f the area of one flange.

The study attempted to relate the inelastic hinge capacity to the optimum yielded length, for sections having flange slenderness ratios, b/t, defined by the equation:

$$\left(\frac{b}{t}\right)^2 = \frac{12.64}{3 + \frac{\sigma_u}{\sigma_y}} \cdot \frac{1}{\varepsilon_y} \cdot \frac{1}{1 + \frac{h}{5.2}} \tag{2.3}$$

Where σ_u represents the ultimate strength of the material and h represents the ratio E/E_{st}.

The predictions of the optimum yielded length given by Equation 2.3 agree qualitatively with experimental results of tests on beams and stub columns [8]. Based primarily on the results of stub column tests, Haaijer and Thurlimann concluded that the critical b/t

ratio for wide-flange beams of A-7 steel was 17 . These experimental results form the basis for the C.S.A. [9] and A.I.S.C. [10] code limitations for compact sections.

Lukey and Adams, in 1967, reported the results of an experimental investigation of the influence of the flange slenderness ratio on the rotation capacity of members subjected to moment gradient [2]. Three series of tests were performed on rolled wide-flange beams of G40.12 steel, having a range of b/t values from 14.0 to 19.4 . The specimens were simply supported and subjected to a concentrated load at midspan. The unbraced slenderness ratio, L/r_y , was approximately 35 for all specimens.

The results of the Series B tests, taken from this study, are given in FIG. 2.2 [2]. This figure shows that a wide range of rotation capacities, $R = \theta/\theta_p - 1$ (where θ is the rotation corresponding to M_p on the unloading branch of the curve), were observed. The rotation capacities were limited by the inelastic buckling of the compression flange, which triggered large lateral deformations of the unbraced span and eventual unloading of the member. As expected, the rotation capacity decreased as the flange slenderness ratio (b/t) was increased.

The inelastic lateral-torsional buckling problem has received only a limited amount of study. Lay and Galambos analyzed the lateral buckling model shown in FIG. 2.3 [3]. The model consists of a column composed of the compression flange tee, laterally unbraced over a length, L , and subjected to a uniform axial load, $\sigma_y A/2$. The yielded length of the column is τL , and the lateral restraint at the yielded end is neglected. The rotational restraint provided by the adjacent

span at the elastic end of the beam is represented by the spring constant SEI_{yy}/L .

It is assumed that the extent of yielding exerts a greater influence on the lateral buckling load than does the variation in stress, therefore, the stress is assumed to remain constant at the yield stress.

The solution of the differential equation describing the lateral buckling of this model results in a relationship between λ and τ . A comparison of the lateral and local buckling solutions shows that the value of λ corresponding to simultaneous local and lateral buckling is approximately 0.7 . However, in this region the solutions are ill-defined. The present test series include beams having values of λ greater than 0.7 . Therefore theoretical and experimental work related to the lateral buckling of wide-flange beams subjected to moment gradient is of importance in this study.

Adams, Lay, and Galambos have reported the results of tests on three simply supported beams subjected to loads producing a moment gradient [5]. The tests were performed on A441 steel wide-flange members having a nominal yield stress of 50 ksi. The unbraced slenderness ratio, L/r_y , was varied for the three tests and also, of necessity, the moment gradient. As the beams were loaded, the lateral deflections remained relatively small until local buckling was induced in the compression flange. Once local buckling had occurred the lateral deflections increased rapidly and eventually unloading of the member was observed. These tests do not provide sufficient information to delineate the influence of bracing spacing on the rotation capacity.

Massey and Pitmann performed an analytical study of the inelastic lateral buckling of simply supported beams subjected to a

concentrated load at midspan [11]. Lateral bracing was provided at the reaction points but not at the load point. An energy solution was used to predict the inelastic lateral-torsional buckling load. In the inelastic portion of the beam, the stiffnesses were reduced linearly to account for the influence of yielding. The predictions were compared to the results of experiments performed on small scale model I - sections. The agreement was generally good. However these results cannot be applied directly to the present investigation because of the difference in the lateral restraint conditions.

An analytical study, by White, has been performed on the lateral-torsional buckling of wide-flange members composed of structural carbon (A-7) steel [4]. The loading on the member was restricted to in-plane end moments.

The inelastic behavior was examined first by analyzing a member which was completely strain-hardened. The results indicated that the critical buckling length was principally dependent upon the warping torsional resistance of the beam, while the St. Venant torsional resistance introduced slight modifications. The effects of moment gradient, extent of strain-hardening and boundary conditions were systematically considered and solutions were obtained for the various cases. The finite difference technique was used to express the differential equations, with the resulting algebraic equations being solved numerically. The results of this study were adjusted to form the basis of a design procedure [4].

The results of recent analytical and experimental investigations have attempted to define the effects of flange slenderness

on the rotation capacity of short beams. However, additional information regarding the effects of moment gradient and lateral bracing spacing is required before design provisions can be formulated.

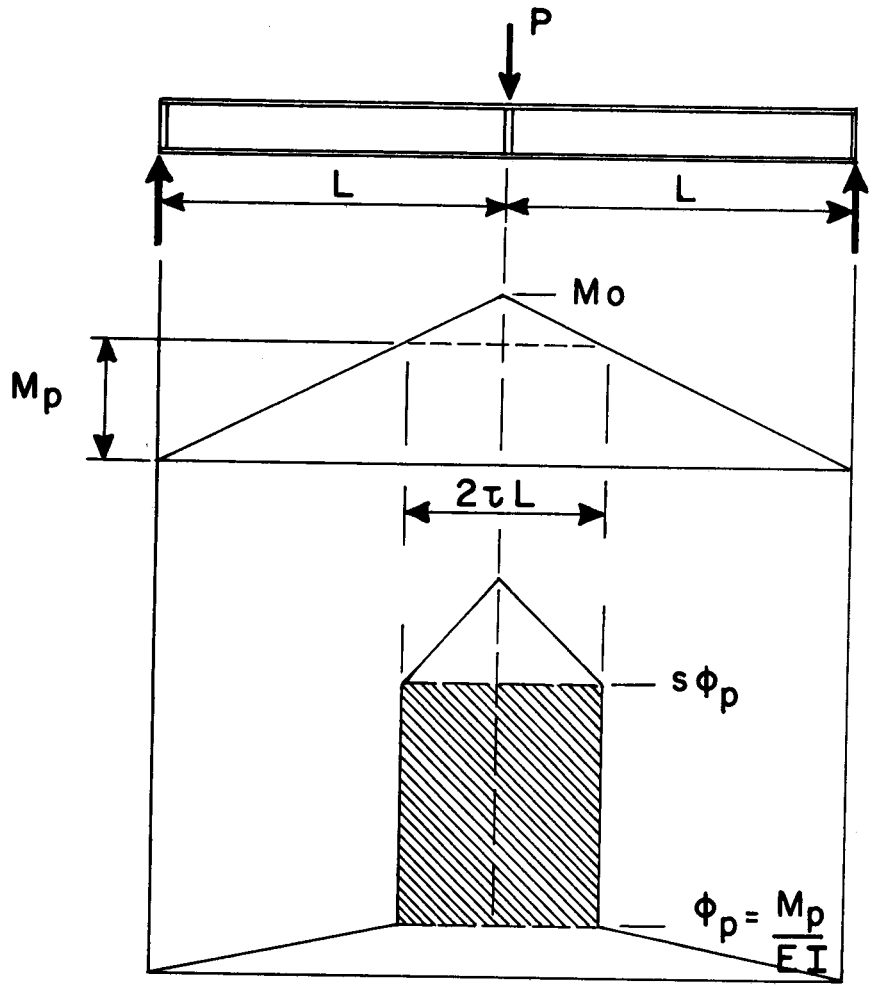

FIGURE 2.1 SIMPLY SUPPORTED WIDE-FLANGE BEAM

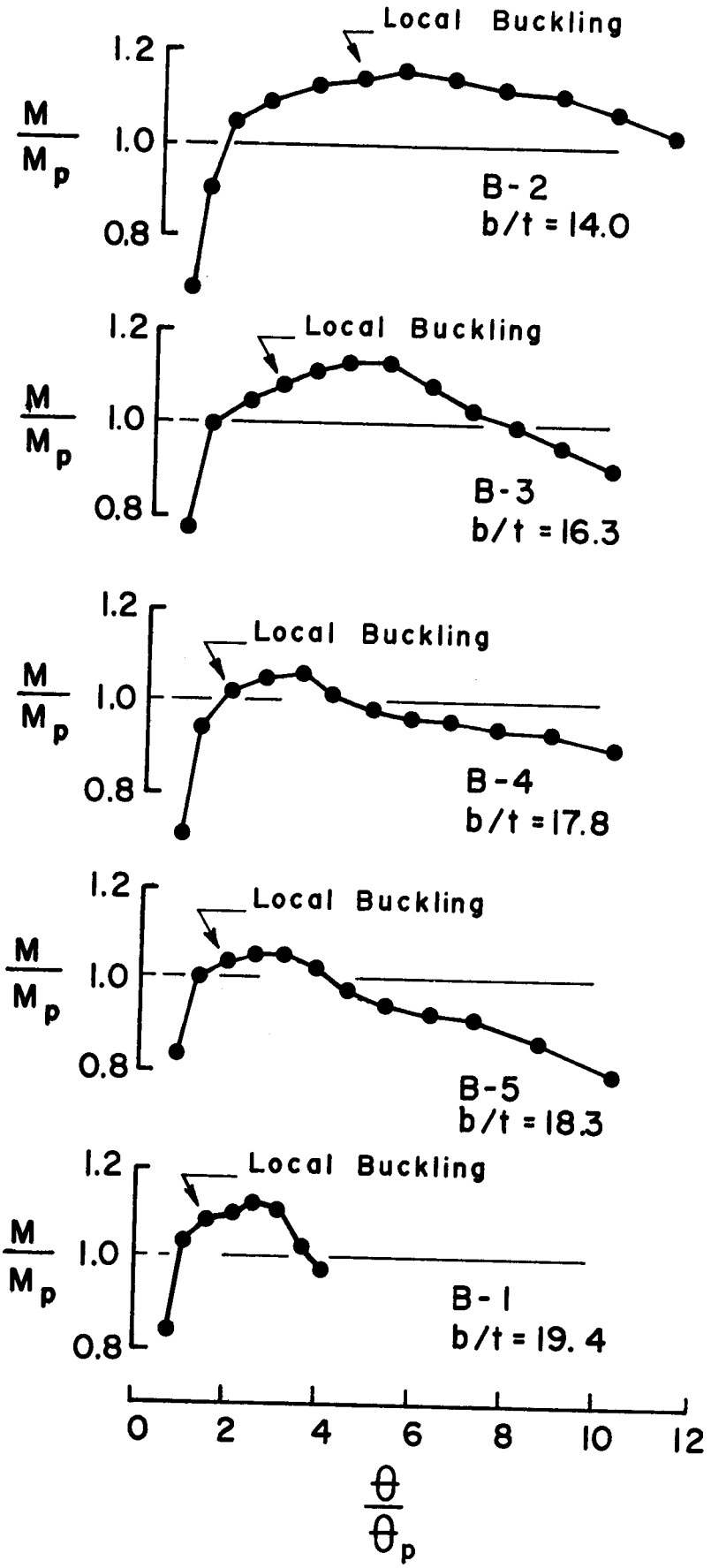

FIGURE 2.2 SERIES B MOMENT-ROTATION RELATIONSHIPS

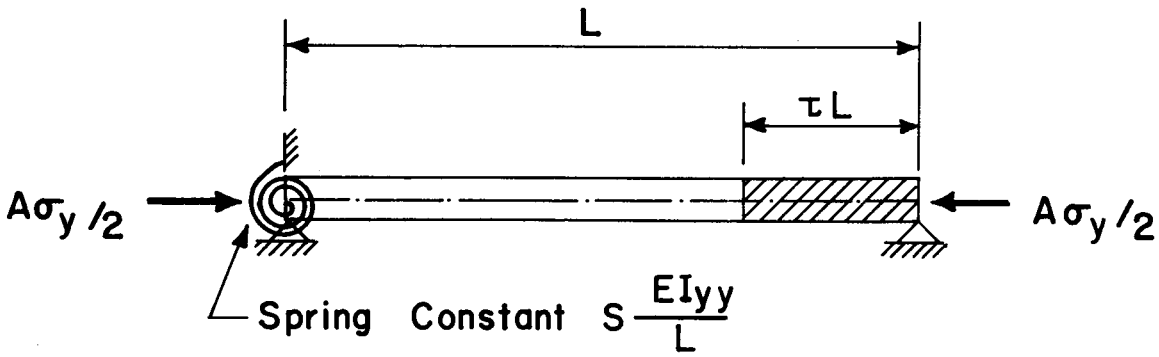

FIGURE 2.3 LATERAL BUCKLING MODEL

CHAPTER III

EXPERIMENTAL PROGRAM

Scope

The experimental program consisted of two series of tests on rolled wide-flange beams of CSA-G40.12 steel [12]. The six lengths used for the test series had been cold-straightened by rotarizing and all lengths were rolled from the same heat [13].

The testing arrangement is shown schematically in FIGS. 3.1(a) and (b). The test beams were simply supported and subjected to a concentrated load at midspan, producing the bending moment distribution shown. The maximum moment, $M = PL/2$, occurred under the load. Lateral bracing was provided at midspan, at the two reaction points, and (for specimens; D-2, D-4, E-2 and E-4 only) at two intermediate locations.

A summary of the specimen dimensions is given in TABLE 3.1. The depth, d, flange width, b, flange thickness, t, web thickness, w, support length, L, and bracing length, L', were determined by measuring the specimens used in the test program.

Each of the two series, D and E, indicated in TABLE 3.2 was chosen to provide a particular flange slenderness ratio (b/t). The desired flange slenderness ratio was obtained by milling down the flange width to the required dimension. The weak axis slenderness ratio

(L/r_y) of the beam was varied within each series by increasing the support length, L. To vary the moment gradient independently of the lateral bracing spacing, the unbraced length, L', was made smaller than the support length, L, as shown schematically in FIG. 3.1(b).

Material Properties

The chemical composition for the material is given in TABLE 3.3 along with the mill test results. These conform to the CSA-G40.12 specification [12].

TABLE 3.4 summarizes the material properties obtained from laboratory tension tests performed on specimens cut from each of the six lengths. The locations from which the coupons were taken are shown in the inset. In this table σ_y denotes the static yield stress, σ_u denotes the ultimate stress, and ε_y is the calculated yield strain corresponding to a modulus of elasticity, $E = 29{,}600$ ksi. ε_{st} is the measured strain at the onset of strain-hardening and E_{st} is the strain hardening modulus [2].

The residual stress distribution over the cross-section is shown in the inset to TABLE 3.4. This distribution is typical for rotarized beams [13].

Testing Arrangement

FIGS. 3.2 and 3.3 show an overall view of the test setup. The arrangement has been described in detail in a previous report [2]. The specimens were tested as simply-supported beams, with the reaction forces taken by hanger rods. The rods were connected to a reaction beam attached to the laboratory floor. Web stiffener plates were welded to all

specimens at the supports and at midspan and also, in some cases, at intermediate brace locations.

The concentrated load was applied by means of a hydraulic ram and transmitted to the beam through a box bolted to the midspan web stiffeners. The box was constructed to contact the specimen only at the stiffeners, and to provide ample clearance for buckling of the compression flange. Hydraulic pressure to the ram was provided by an air-driven pump, and regulated by adjustment of the air pressure and hydraulic line valves at a control panel [2].

For all test specimens lateral braces were provided at the two reaction points and at midspan, as shown in FIG. 3.2. However for some test beams, as indicated in FIG. 3.3, additional lateral braces were provided at two intermediate locations between the midspan and the reaction points. Lateral support at the reaction points was provided by steel rods bolted in a horizontal position between the testing frame and the stiffener plates, as shown in FIG. 3.2. At midspan and at the intermediate locations the articulated bracing mechanism shown in FIG. 3.3 was used.

FIG. 3.4 shows the instrumentation used in the tests. The applied loads were determined by monitoring the strains in the two reaction support rods which had been previously calibrated in a testing machine. The vertical deflection at midspan was measured by means of a dial gage. Support settlements were also measured using dial gages, and the appropriate adjustment made to obtain the net vertical midspan deflection. Rotation gages were attached to the beam ends to measure the rotations at the supports. Lateral movements of the compression flange were measured by means of dial gages placed horizontally between

the beam and the testing frame. For test specimens braced as shown in FIG. 3.2 lateral movements were measured at the beam quarter-points. Lateral movements for beams with intermediate lateral braces (FIG. 3.3) were measured at locations halfway between midspan and the intermediate braces. The relative vertical movements of the tension and compression flanges were measured near the midspan of the beam by a dial gage placed between the flanges in a series of prepunched gage points.

The entire specimen was whitewashed before each test to aid in observing the progression of yielding.

Test Procedure

In the initial elastic range of the test, the specimen was deformed by increasing the hydraulic ram pressure to give predetermined load values. The load was maintained at each of these values until all readings had been taken.

After yielding had occurred, the loading procedure was to increase the midspan deflection to predetermined values; the flow of hydraulic fluid to the ram was then closed off for a five minute stabilization period before readings were taken. In addition to the instrument readings mentioned in the previous section, visual observations and measurements of the progression of yielding, local buckling and lateral buckling were recorded for each increment.

The specimen was deformed well into the unloading range using the above procedure. The ram pressure was then reduced in several increments to trace the elastic unloading curve.

Test	d (in)	b (in)	t (in)	w (in)	L' (in)	L (in)
D-1	7.94	2.654	0.190	0.182		34.8
D-2	7.94	2.656	0.189	0.182	19.1	51.4
D-3	7.94	2.657	0.191	0.182		52.1
D-4	7.94	2.658	0.193	0.185	42.6	73.0
D-5	7.94	2.658	0.192	0.185		44.7
D-6	7.93	2.641	0.188	0.183		17.4
E-1	7.94	3.461	0.192	0.189		48.8
E-2	7.93	3.460	0.189	0.182	27.6	73.2
E-3	7.93	3.461	0.189	0.182		73.2
E-4	7.94	3.461	0.188	0.182	59.8	102.5
E-5	7.93	3.461	0.188	0.182		62.8
E-6	7.93	3.463	0.189	0.183		24.4

TABLE 3.1 SECTION DIMENSIONS

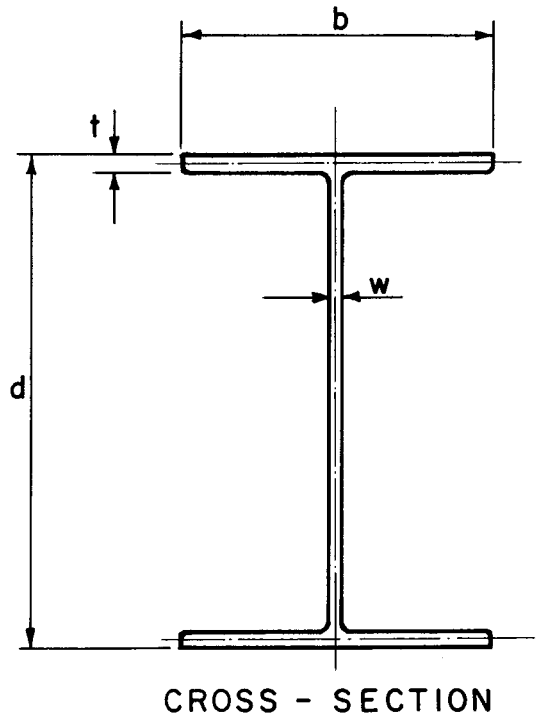

CROSS - SECTION

Test	d/w	b/t	L'/r_y	L/r_y
D-1	43.6	14.0		69.6
D-2	43.6	14.1	38.2	102.9
D-3	43.6	13.9		103.9
D-4	42.9	13.8	85.0	145.7
D-5	42.9	13.8		89.4
D-6	43.3	14.0		35.2
E-1	42.0	18.0		70.2
E-2	43.6	18.3	39.5	104.8
E-3	43.6	18.3		104.8
E-4	43.6	18.4	85.7	146.9
E-5	43.6	18.4		90.0
E-6	43.4	18.3		34.9

TABLE 3.2 TEST PROGRAM

Physical Properties			Chemical Composition %				
Yield Stress (ksi)	Ultimate Stress (ksi)	Elongation %	C X100	Si X100	Mn X100	P X1000	S X1000
57.6	68.8	19	15	7	46	6	23

TABLE 3.3 CHEMICAL COMPOSITION AND MILL TEST RESULTS

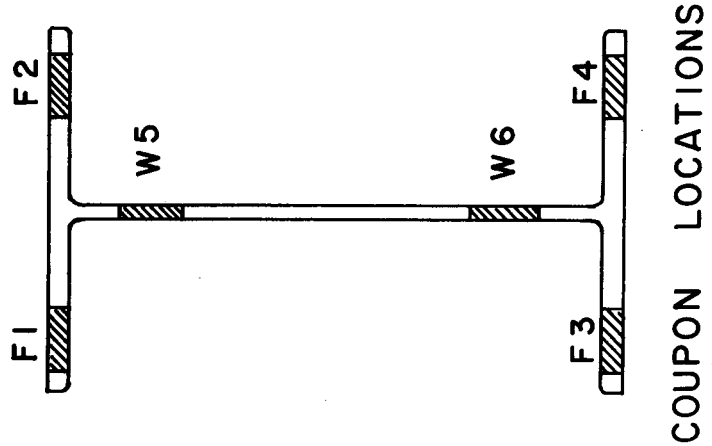

Length	Test	Coupon	σ_y (ksi)	$\varepsilon_y = \sigma_y/E^*$	ε_{st}	E_{st} (ksi)	σ_u (ksi)	Elongation %
A	D-2	F1	40.3	0.00136	0.0214	384	61.4	24.4
	and	F2	43.7	0.00148	0.0208	415	63.0	26.5
	E-5	F3	--	--	0.0218	428	--	22.1
		F4	--	--	0.0220	440	--	23.5
		W5	54.1	0.00183	0.0230	353	69.2	22.3
		W6	55.1	0.00186	0.0228	257	67.4	17.8
B	D-3	F1	42.2	0.00143	0.0156	390	61.9	25.8
	and	F2	45.0	0.00152	0.0207	417	63.3	23.1
	E-1	F3	41.1	0.00139	0.0174	415	61.9	24.6
		F4	46.6	0.00157	0.0181	408	64.0	23.8
		W5	52.7	0.00178	0.0247	466	67.3	19.6
		W6	55.6	0.00188	--	300	68.2	17.6
C	D-1	F1	43.2	0.00146	0.0199	480	62.3	23.4
	and	F2	39.1	0.00132	0.0174	406	60.7	23.3
	E-2	F3	43.7	0.00148	0.0194	369	62.0	26.6
		F4	39.7	0.00134	0.0191	431	61.0	28.1
		W5	54.9	0.00186	0.0237	289	65.6	16.3
		W6	52.3	0.00177	0.0252	286	67.8	19.1

*Note - E taken as 29.6×10^3 ksi

TABLE 3.4 MATERIAL PROPERTIES

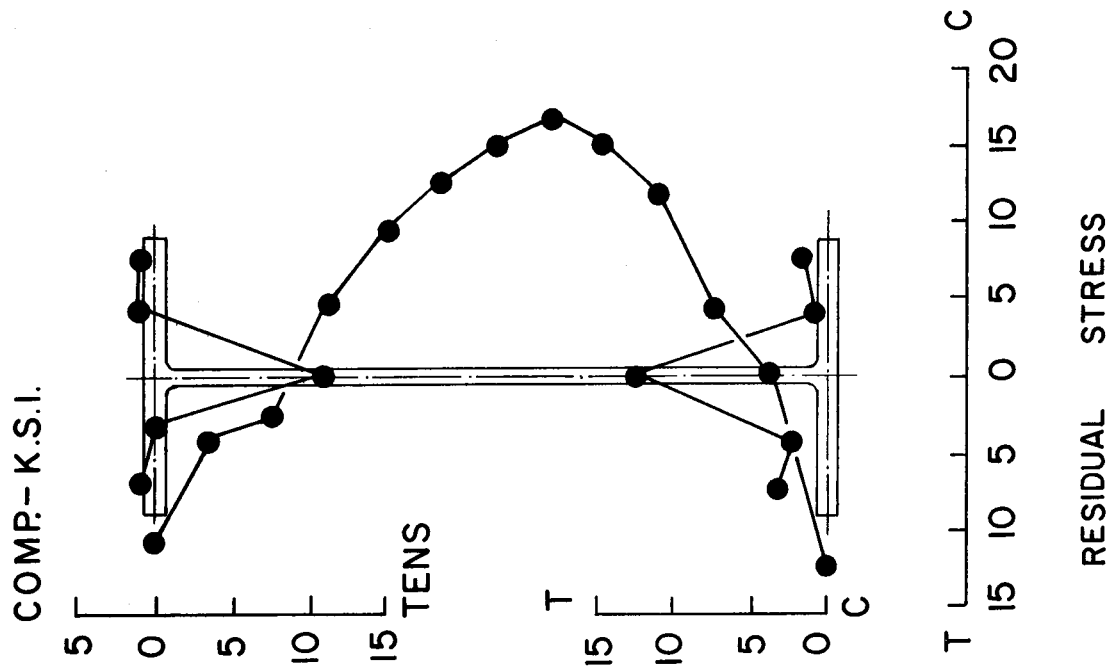

Length	Test	Coupon	σ_y (ksi)	$\varepsilon_y = \sigma_y/E^*$	ε_{st}	E_{st} (ksi)	σ_u (ksi)	Elongation %
D	E-3	F1	44.2	0.00149	0.0165	433	61.7	23.6
	and	F2	38.7	0.00131	0.0188	397	59.7	25.1
	E-4	F3	38.1	0.00129	--	383	58.7	25.0
		F4	42.1	0.00142	0.0148	448	60.6	26.6
		W5	52.5	0.00178	0.0208	335	65.4	19.5
		W6	53.7	0.00182	--	326	66.1	17.6
E	D-4	F1	39.4	0.00133	--	---	60.4	27.8
	and	F2	41.7	0.00141	--	---	60.5	28.0
	D-5	F3	40.1	0.00135	0.0177	341	60.7	25.2
		F4	41.7	0.00141	--	385	60.3	24.0
		W5	55.9	0.00189	--	302	68.8	17.6
		W6	55.0	0.00186	--	---	67.8	19.1
F	D-6	F1	41.8	0.00141	0.0190	378	61.6	26.0
	and	F2	48.1	0.00162	0.0230	377	66.7	26.0
	E-6	F3	40.9	0.00138	0.0222	432	61.8	25.9
		F4	46.4	0.00157	0.0178	422	66.1	22.5
		W5	54.1	0.00183	0.0180	285	66.2	17.1
		W6	56.2	0.00190	0.0184	277	71.2	18.4

*Note - E taken as 29.6×10^3 ksi

TABLE 3.4 MATERIAL PROPERTIES (Cont'd)

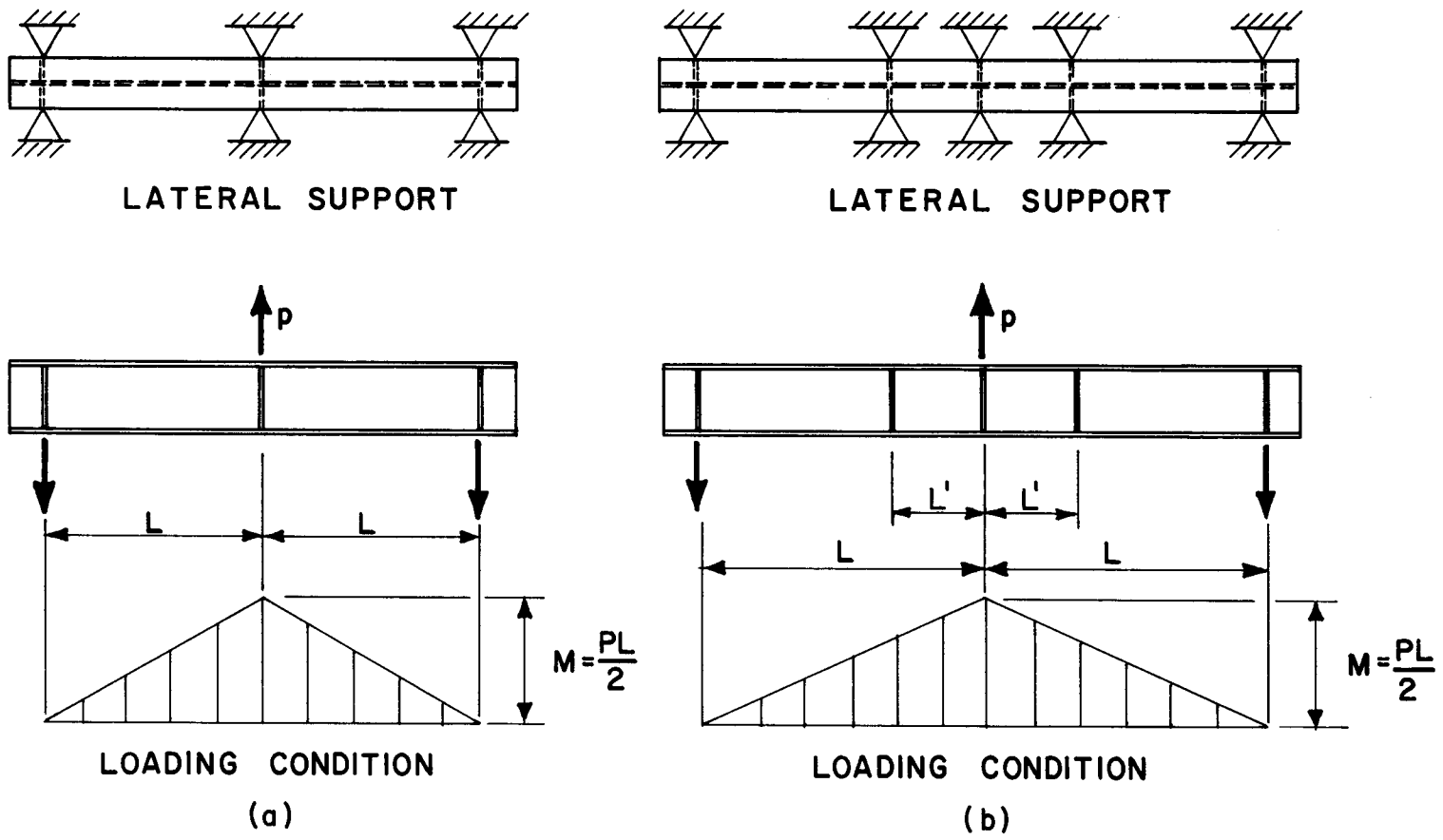

FIGURE 3.1 TESTING ARRANGEMENT

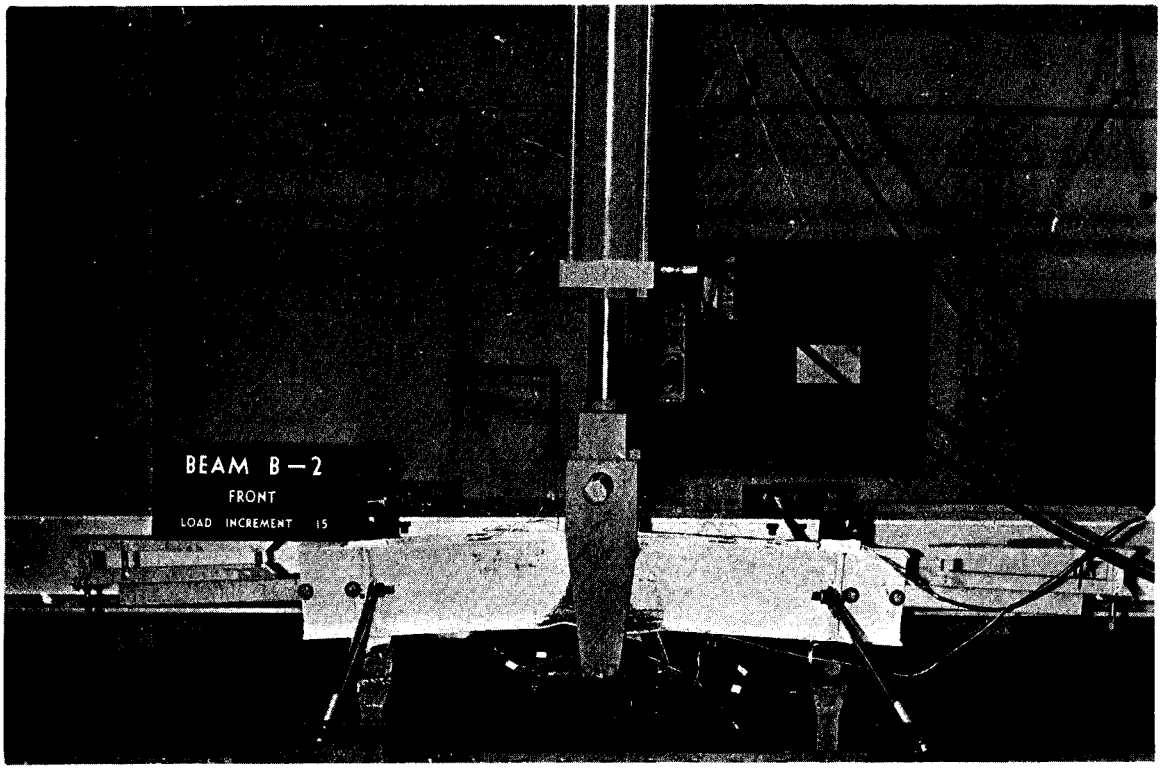

FIGURE 3.2 TEST SETUP - TOP FRONT VIEW

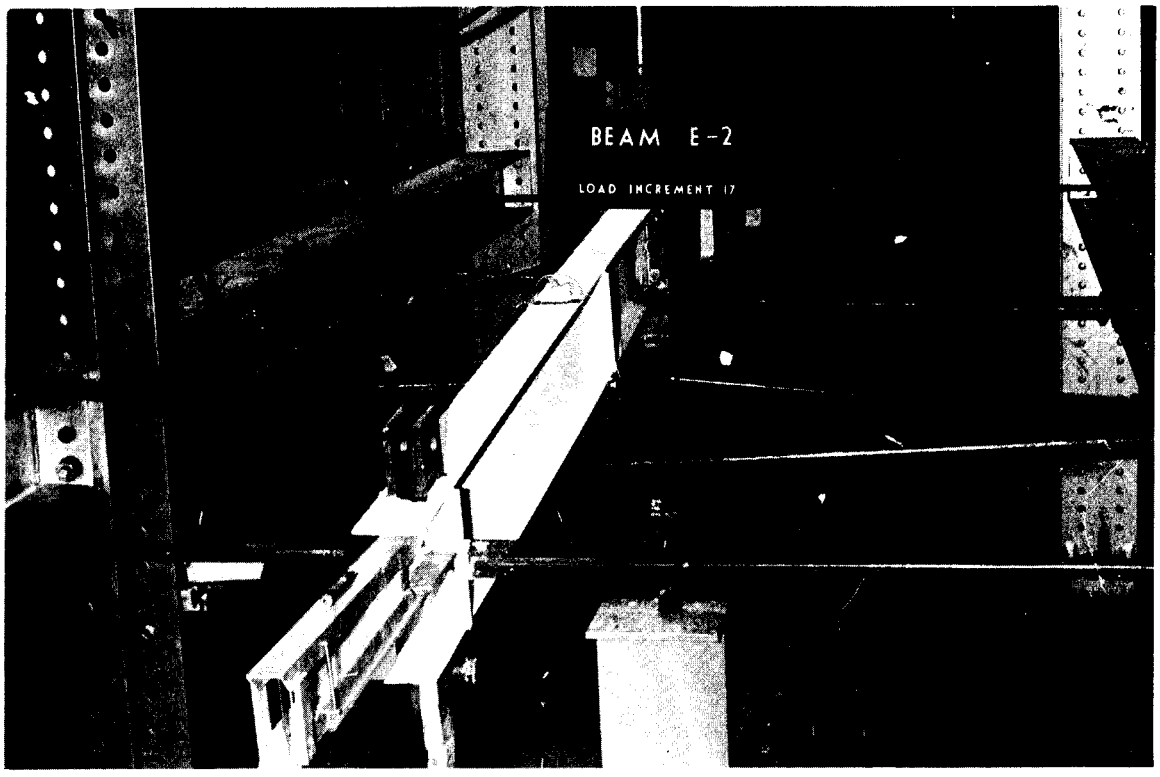

FIGURE 3.3 TEST SETUP - TOP END VIEW

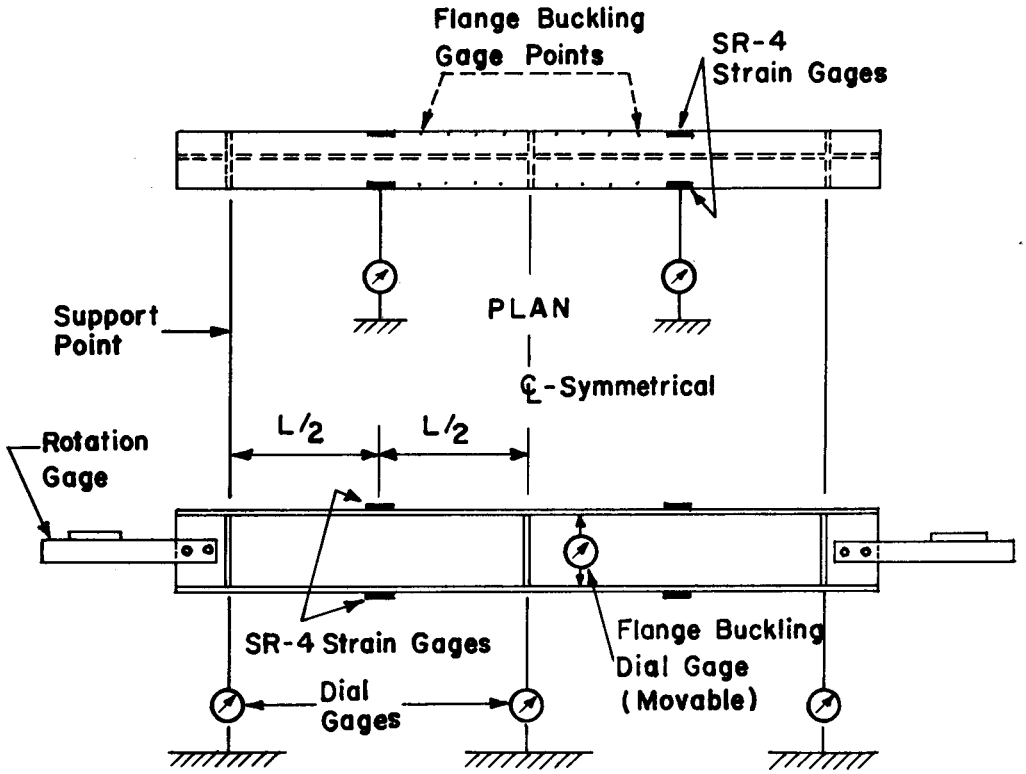

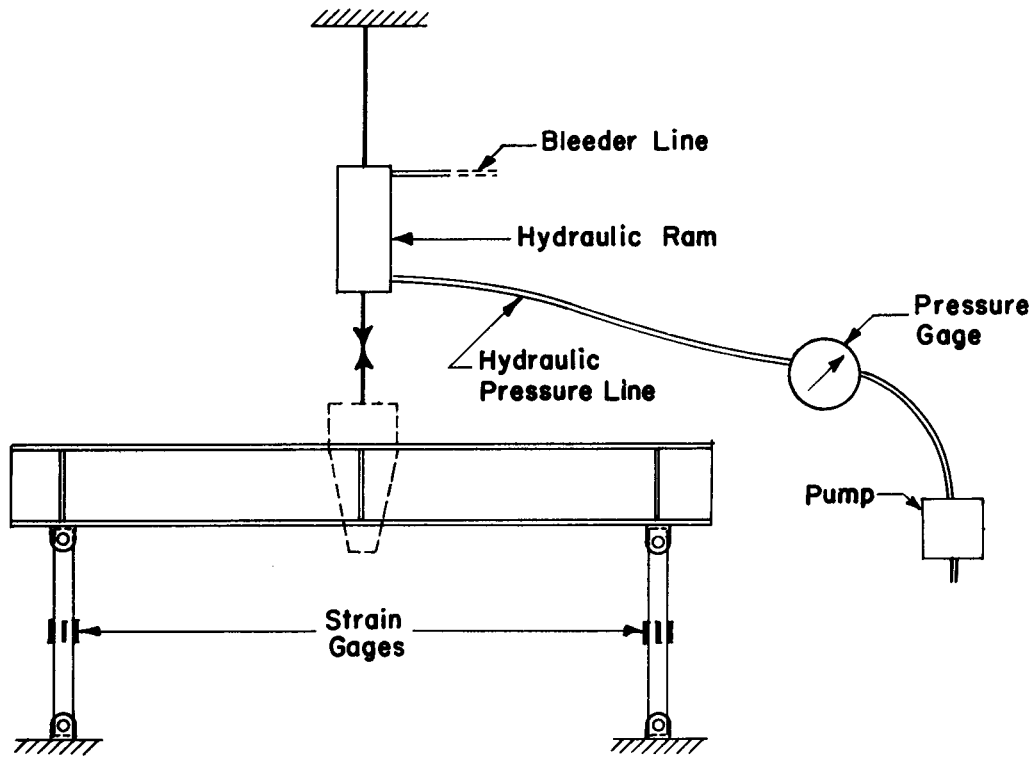

FIGURE 3.4 INSTRUMENTATION

CHAPTER IV

RESULTS

FIG. 4.1 is a graph of midspan moment, M, non-dimensionalized as M/M_p, versus rotation, θ, for beam D-5. M_p was calculated using the measured cross-section dimensions and the flange and web yield stresses obtained from tension tests. $\theta = \theta_L + \theta_R$ is the total of the two measured end rotations (see inset). The behavior predicted by the simple plastic theory is shown by the dashed lines, and the actual behavior as the full lines joining the solid circles. Each solid circle (and adjacent number) represents a stage during the test at which data was recorded.

The member behaved elastically up to Load No. 2. First yielding was observed during the application of Load No. 3, and beyond this stage the rotations increased rapidly. The moment continued to increase beyond M_p and between Load Nos. 4 and 5, lateral deflections were observed visually between bracing points. Beyond Load No. 5 the member unloaded, that is, an increase in deformation was accompanied by a decrease in load (moment). The moment decrease was rapid and was accompanied by local buckling of the compression flange and increasing lateral deformation of the unbraced spans. The local deformations were first observed visually at Load No. 6. Beam E-5, having the same slenderness ratio, but a b/t value of 18.3 (instead of 14.0), behaved in a similar manner. However, the moment

decreased more slowly at first with the decreases becoming more rapid as local deformations increased. Specimens D-5 and E-5 had unbraced slenderness ratios, L/r_y, of approximately 90. Both the observed and theoretical rotations plotted in FIG. 4.1 and all subsequent figures exclude the effects of shear deformations [6].

FIG. 4.2 plots M/M_p versus the vertical deflection at midspan, v, for beam D-5. Again the solid lines represent the actual beam behavior and the dashed lines represent the elastic-plastic prediction. The experimental curve is similar to the M-θ curve of FIG. 4.1.

For beam D-5, local buckling deformations of the compression flange are shown in FIG. 4.3. This figure plots M/M_p versus the out-of-plane displacement of the compression flange tips, δ, at two gage points on opposite sides of the web. The change in distance between the tension and compression flanges was measured with a dial gage, as shown in the inset; this change was taken to represent the out-of-plane displacement of the compression flange tips. The two gage points for which the deflections are plotted are those which had the largest observed deformations. The first evidence of flange displacement at these points occurred at Load No. 6. This coincided with the stage at which local buckling was first observed visually. The local deformations increased rapidly beyond Load No. 6. For this beam, as for others in the test series, the out-of-plane movement was greatest in the direction toward the tension flange.

FIG. 4.4 shows a graph of M/M_p versus the lateral displacements of the compression flange quarter-points, u, (as shown in the inset) for beam D-5. The deformations are non-dimensionalized

as u/b . The first pronounced movement occurred between Load Nos. 4 and 5. At Load No. 6 the local buckling deformations became severe causing the lateral deformations to increase rapidly. The combined lateral and local deformations were accompanied by a decrease in moment capacity. For this beam, the lateral displacement at one of the quarter-points (right) was greater than the other (left) because local buckling occurred primarily on the right side of midspan. A similar situation was observed in a number of the tests, although some did deform almost symmetrically about midspan. In all tests (without intermediate braces) the compression flange deflected laterally into an S shape, as may be seen for the series D specimens in FIG. 4.5.

For specimens D-6 and E-6, with unbraced slenderness ratios of approximately 35 , and for specimens D-1 and E-1, with L/r_y ratios of approximately 70 , the behavior is similar to that described in a previous report [2]. However, for the two longer beams, ($L/r_y = 70$) local buckling was accompanied by larger lateral deflections of the unbraced span. The moment did not increase beyond this stage (as was the case for shorter beams), but instead held constant for a limited rotation before dropping off at a relatively rapid rate.

FIG. 4.6 is a plot of M/M_p versus θ for beam D-3. The unbraced slenderness ratio for this beam was approximately 105 . The member behaved elastically up to Load No. 2. First yielding was observed between Load Nos. 2 and 3 and the moment continued to increase up to Load No. 4. However, during the application of Load No. 5 large lateral deformations were observed and the member began to unload. Between Load Nos. 4 and 6 the moment decreased slowly; after

this stage the decrease became more rapid. No local deformations were observed for beam D-3. The behavior of beam E-3, having the same slenderness ratio, but a b/t value of 18.3 (instead of 13.9), behaved in a similar fashion except that the maximum moment exceeded M_p . In addition, small local deformations were observed at the peak of the M-θ curve.

FIG. 4.7 shows a graph of M/M_p versus the lateral displacements of the compression flange quarter-points for beam D-3. The first pronounced movement occurred during the application of Load No. 5. Beyond this point lateral deformations increased rapidly and were accompanied by a drop in moment capacity. For this beam the lateral displacements of the quarter-points were considerably greater than those of beam D-5. FIG. 4.8 shows the lateral deformations at various loading increments. The numbers shown in the photographs correspond to the load numbers shown in FIG. 4.6.

FIG. 4.9 is a plot of M/M_p versus θ for beam E-2. The half-span, L , was approximately 105 r_y and the distance from the load point to the intermediate brace, L' , was approximately 39 r_y . The member behaved elastically up to Load No. 3. First yielding was observed between Load Nos. 3 and 4. The moment continued to increase beyond M_p and, at Load No. 7, the local deformations of the compression flange and the lateral deflections of the unbraced span were first observed visually. Lateral deflections were measured half-way between the load point and the intermediate lateral braces. The increase in moment continued up to Load No. 10. Beyond this stage the member gradually unloaded. Beam D-2, having the same half-span and unbraced length, behaved in a similar manner. This behavior was also typical for

specimens E-4 and D-4 in which the half-span was approximately 147 r_y and the unbraced length was approximately 85 r_y . However, for these specimens large lateral deformations between braces were observed visually before local deformations of the compression flange were observed. Once local deformations had occurred the member unloaded. During unloading the lateral deformations increased rapidly.

The experimental moment-rotation relationships for the 12 beams tested are summarized in FIGS. 4.10, 4.11 and 4.12. In these figures, M/M_p is plotted against the dimensionless rotation parameter, θ/θ_p , $(\theta_p = M_p/EI)$.

In Series D and E the unbraced slenderness ratios tested ranged from approximately 35 to approximately 105 . The flange slenderness ratios were approximately 14.0 for Series D, and 18.3 for Series E. These two b/t values were chosen to define the effect of flange slenderness on the rotation capacity, for various unbraced lengths. FIGS. 4.10 and 4.11 show the large variations in rotation capacity which occurred within this range of L/r_y values.

FIG. 4.12 shows the beams tested in Series D and E in which the unbraced length, L' , was somewhat smaller than the half-span, L (as shown in FIG. 3.1). These tests were chosen to separate the influence of moment gradient from that of the unbraced slenderness ratio, on the rotation capacity of the members.

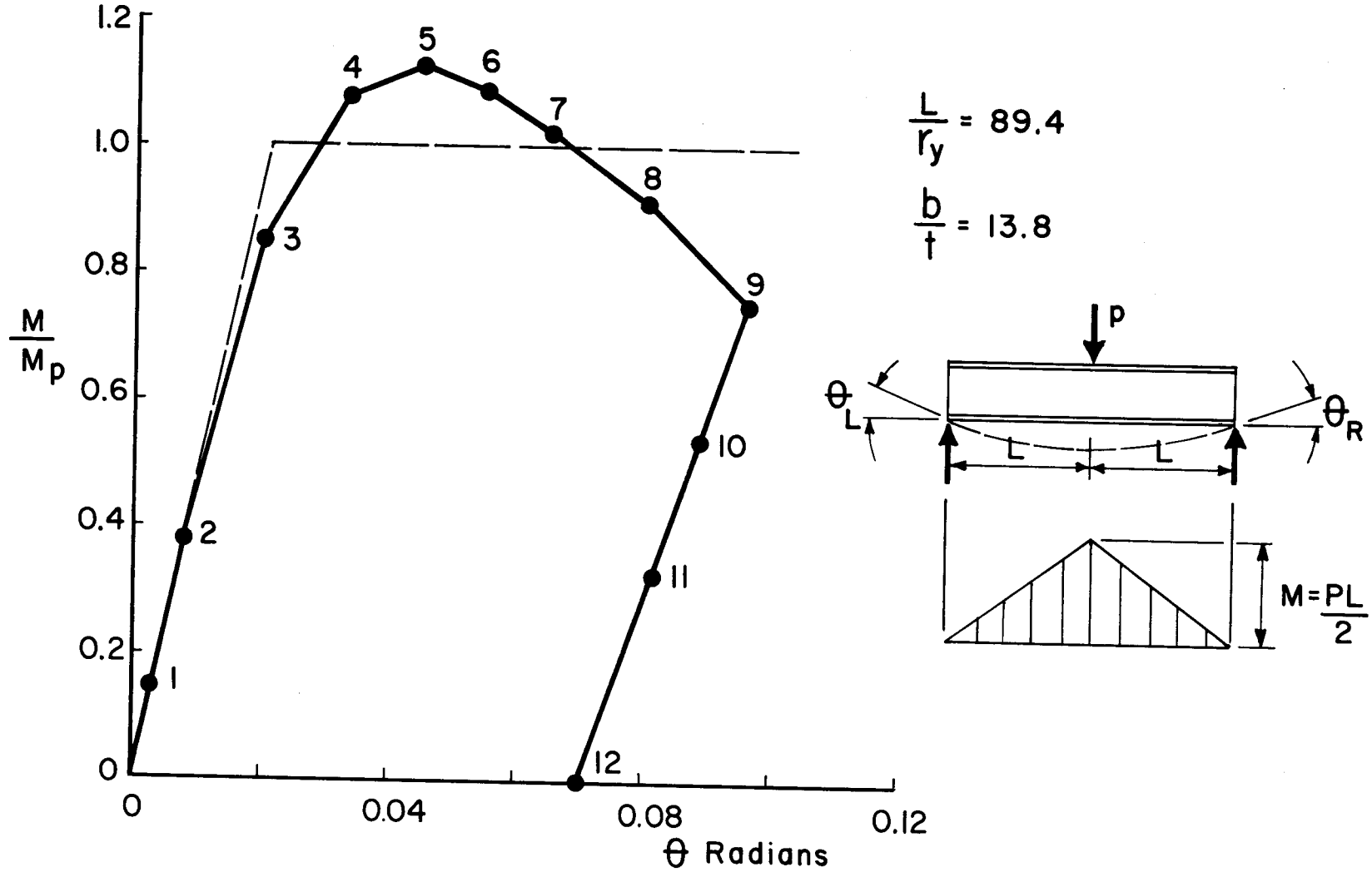

FIGURE 4.1 MOMENT-ROTATION RELATIONSHIP - BEAM D-5

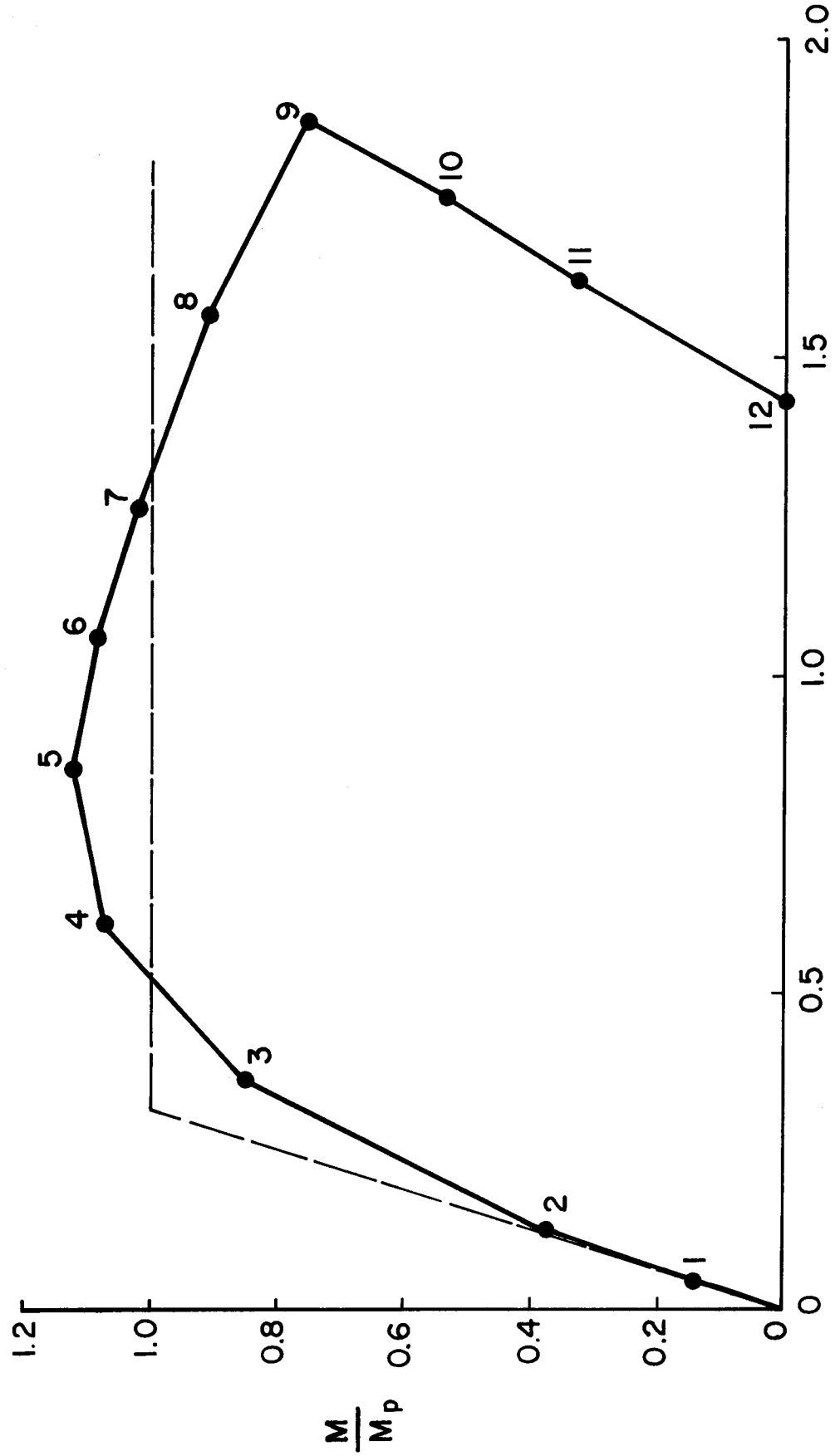

FIGURE 4.2 MOMENT-DEFLECTION RELATIONSHIP - BEAM D-5

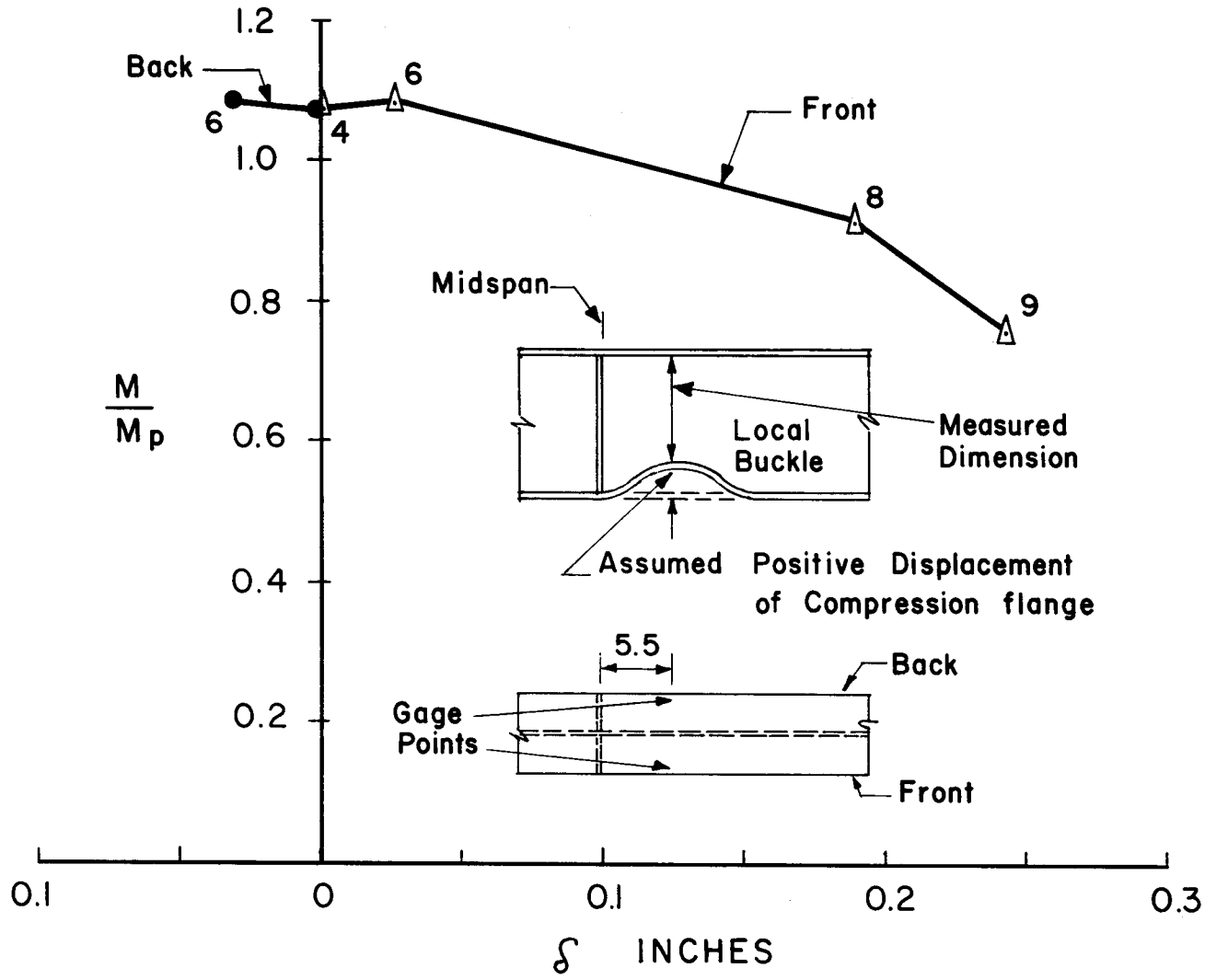

FIGURE 4.3 LOCAL BUCKLING DEFORMATIONS - BEAM D-5

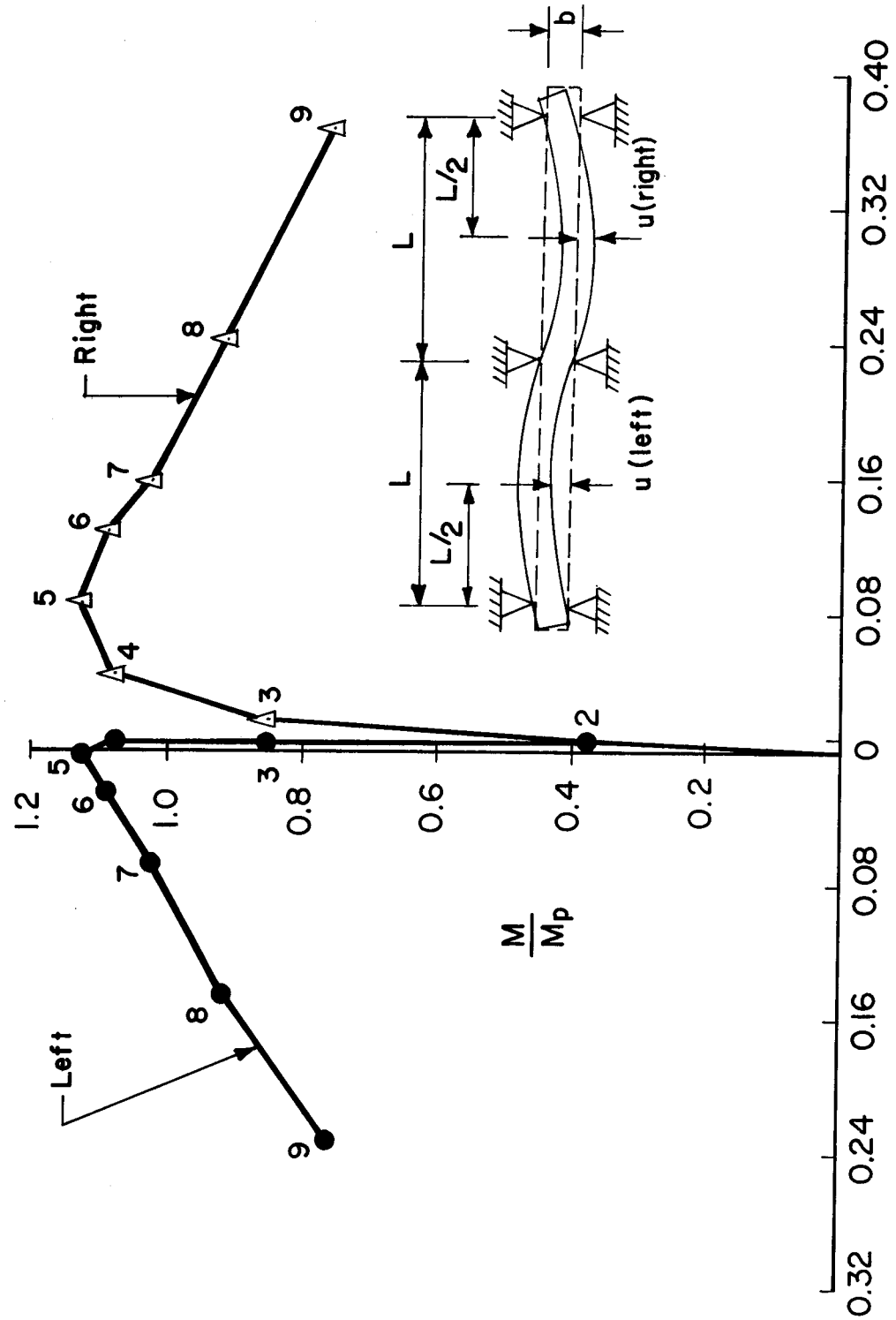

FIGURE 4.4 LATERAL DEFLECTIONS - BEAM D-5

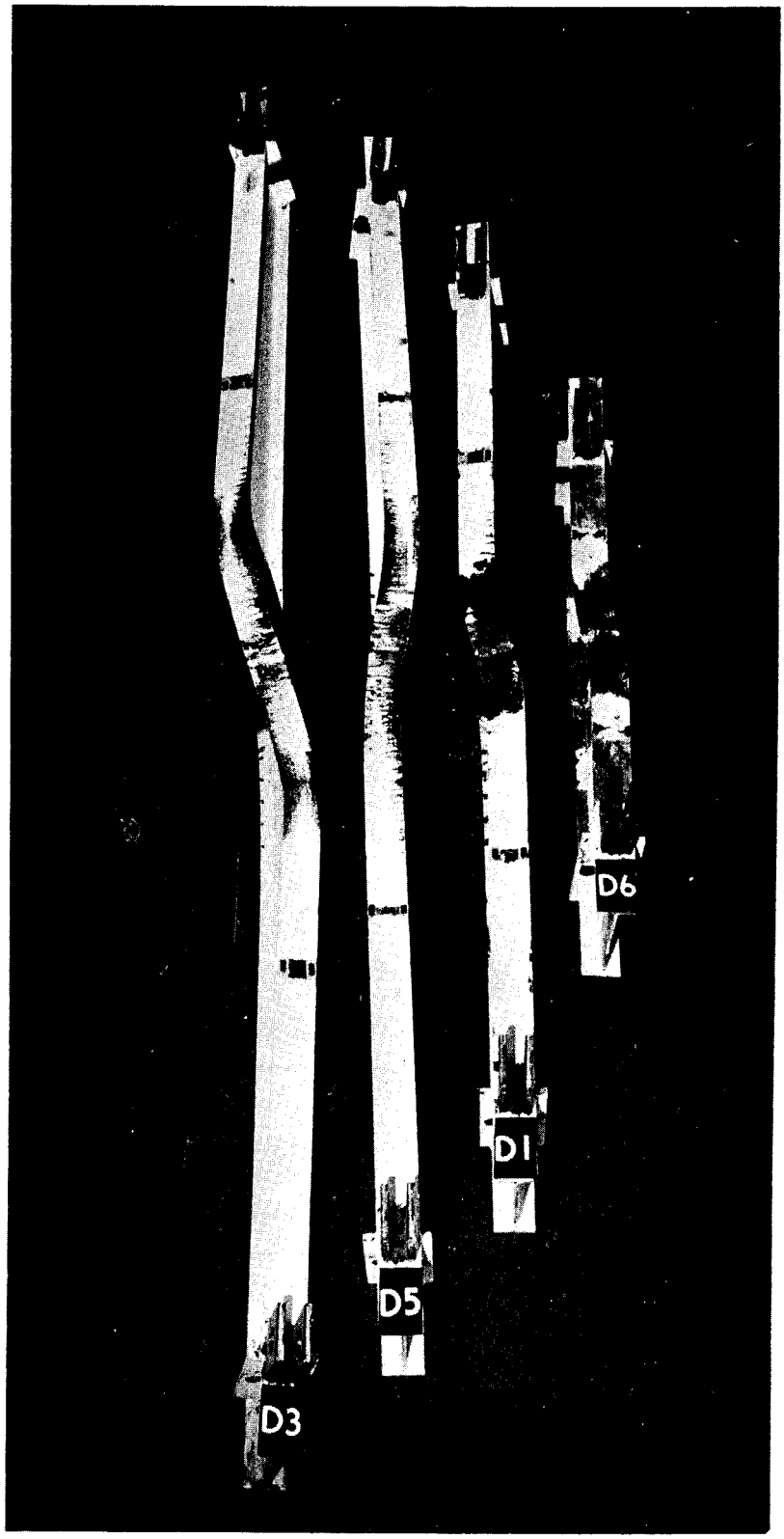

FIGURE 4.5 SERIES D SPECIMENS AFTER TESTING

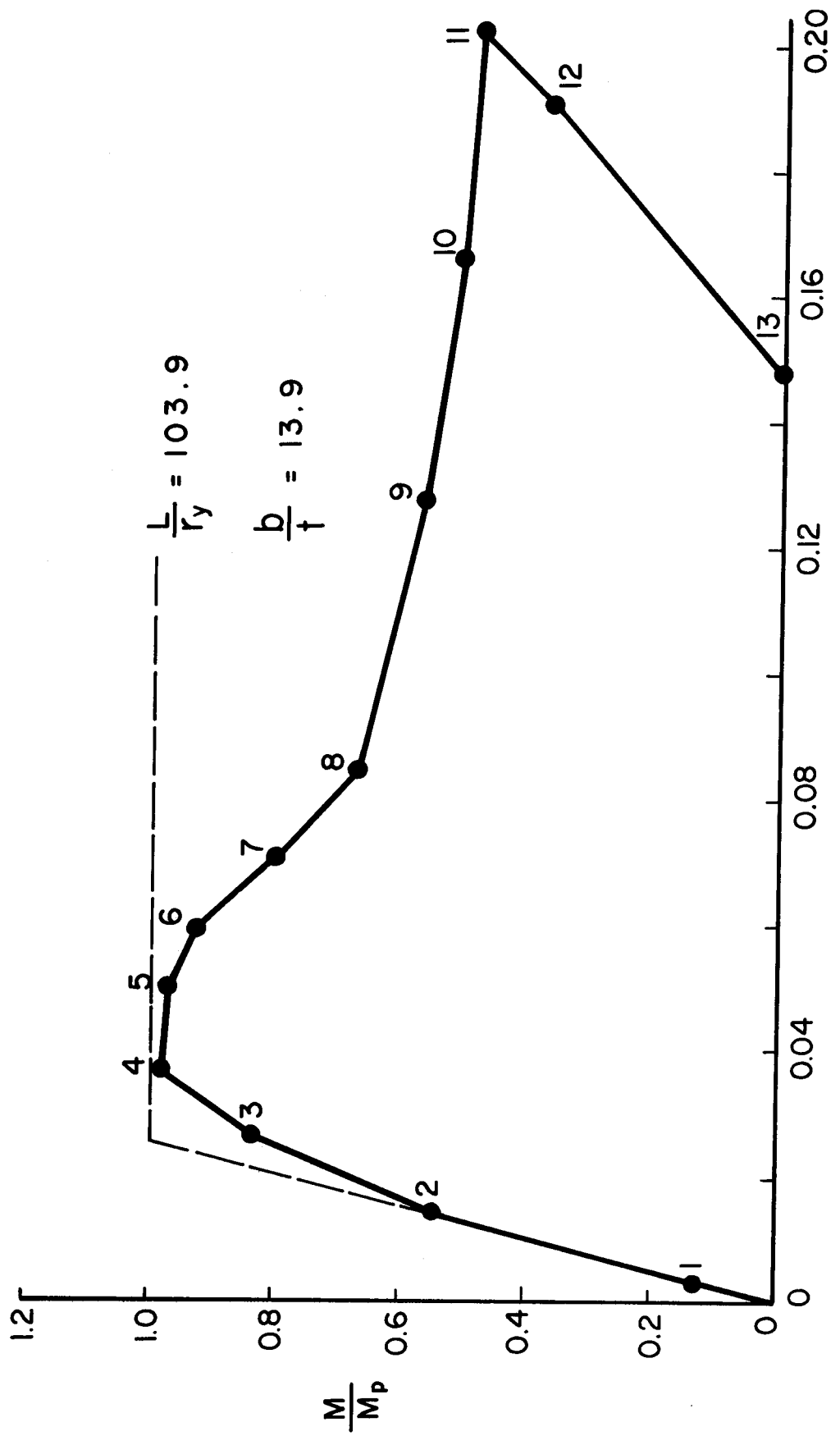

FIGURE 4.6 MOMENT-ROTATION RELATIONSHIP - BEAM D-3

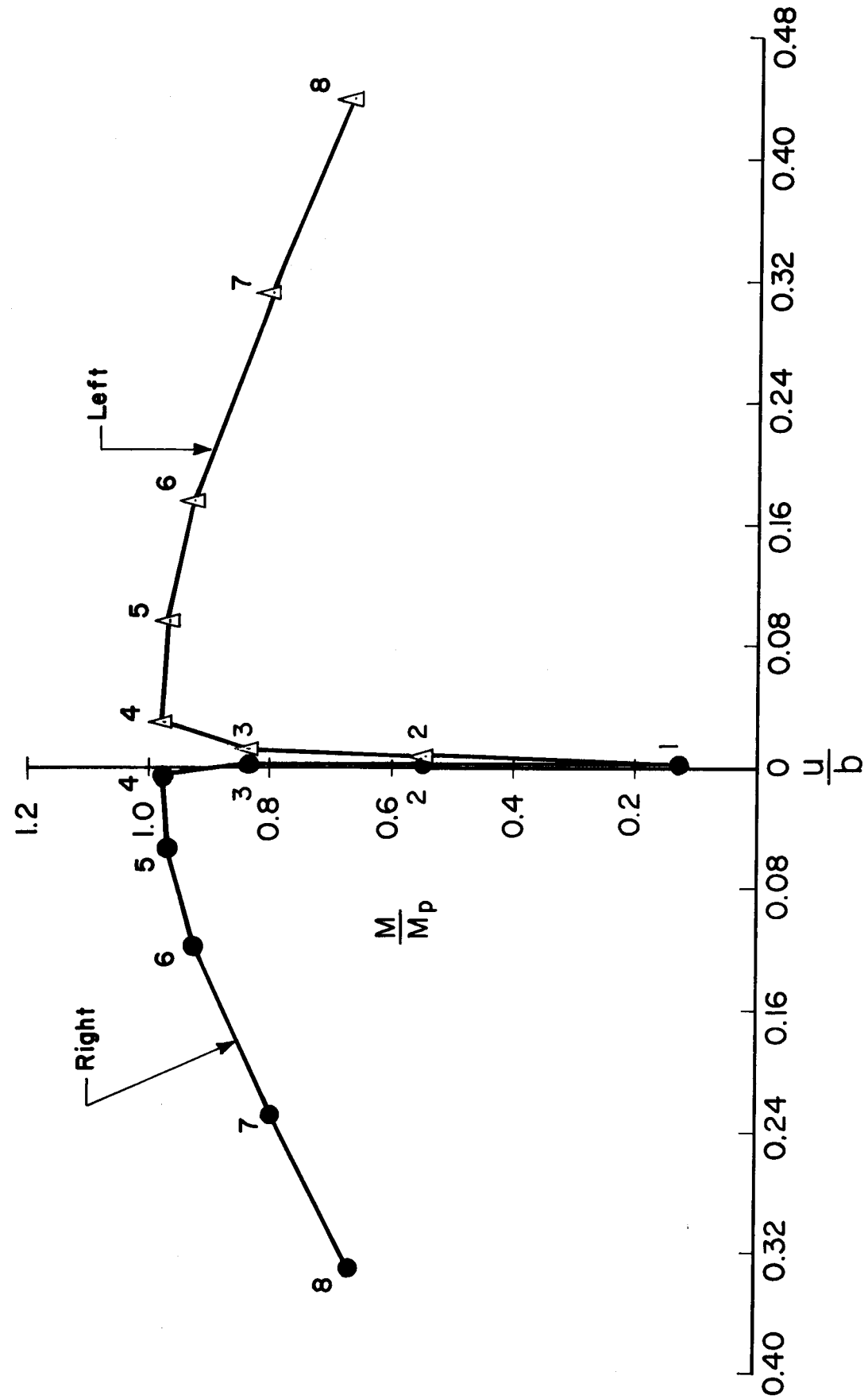

FIGURE 4.7 LATERAL DEFLECTIONS - BEAM D-3

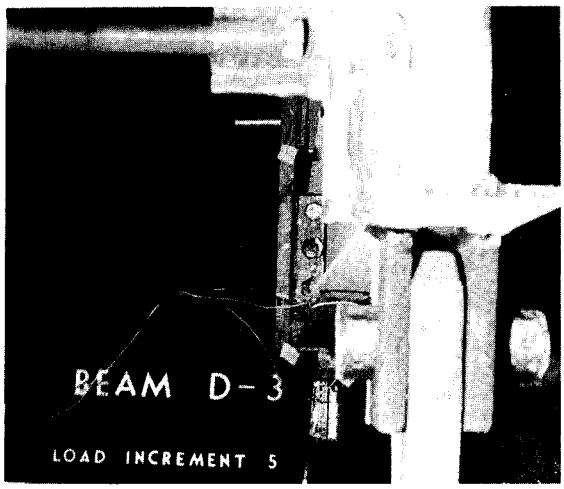

(a)

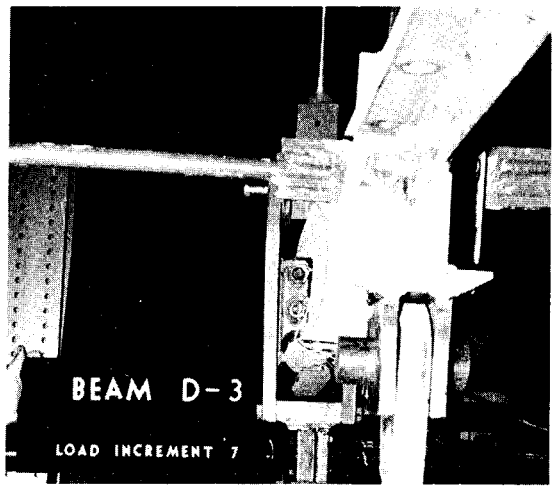

(b)

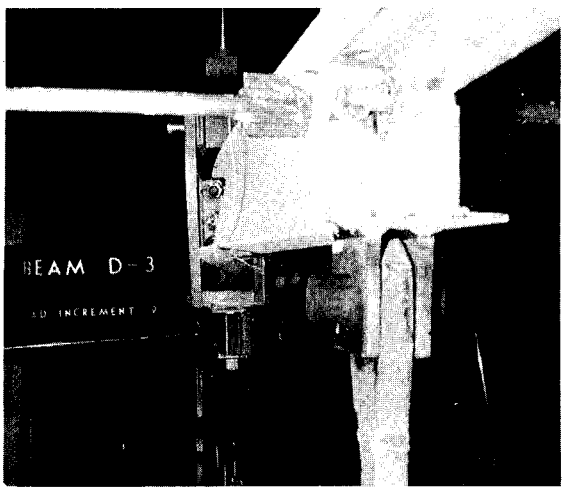

(c)

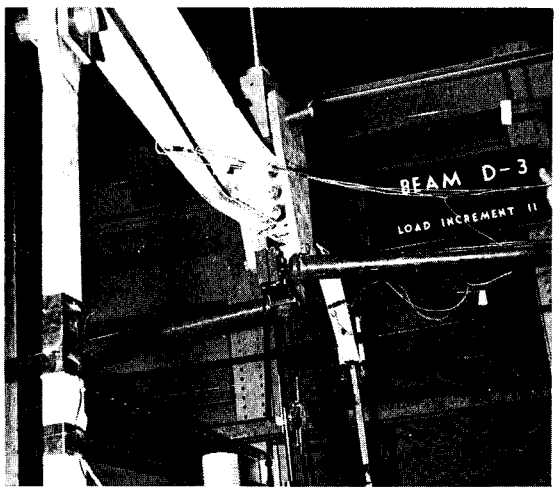

(d)

FIGURE 4.8 BEAM D-3 DURING TESTING

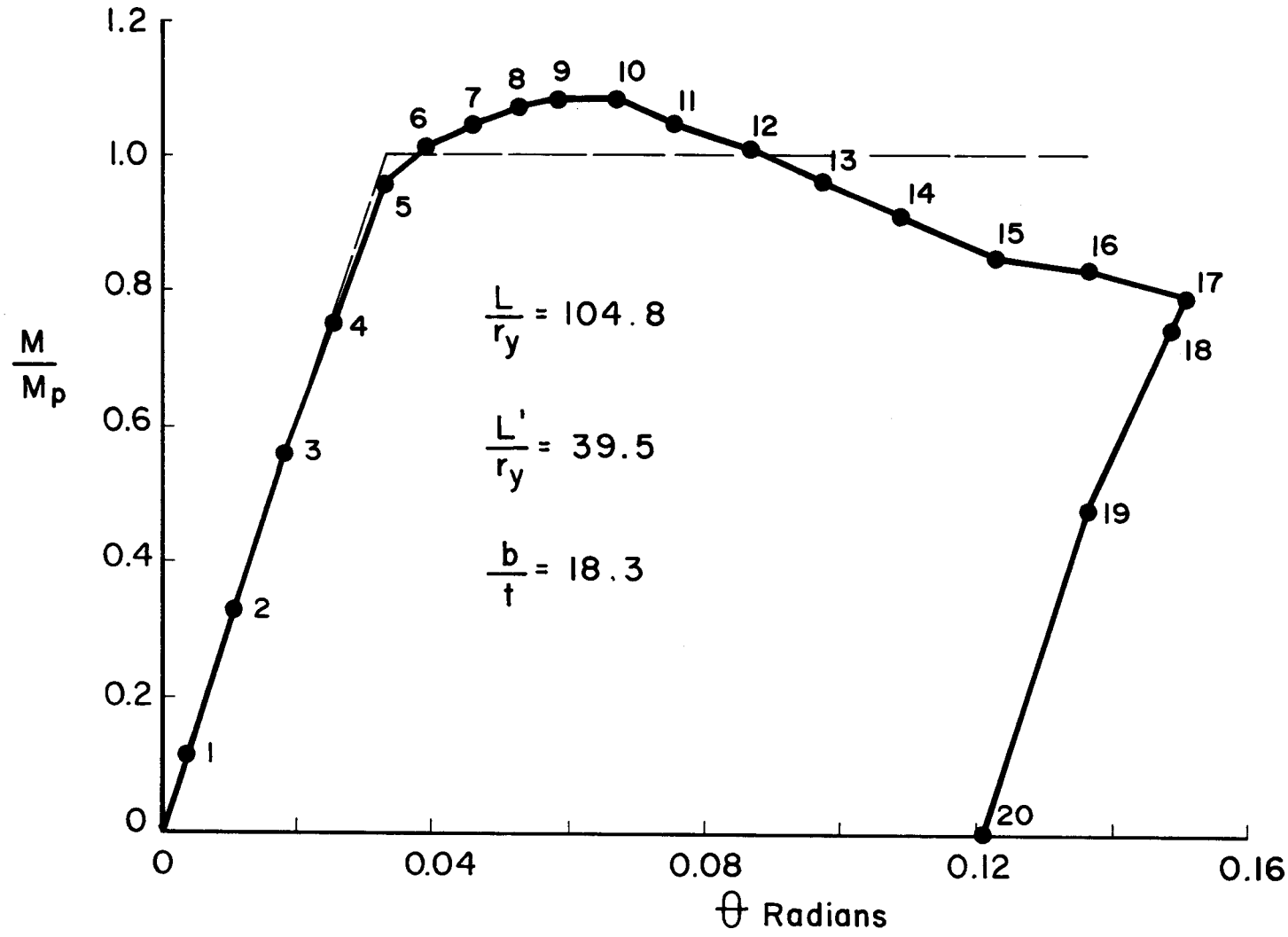

FIGURE 4.9 MOMENT-ROTATION RELATIONSHIP - BEAM E-2

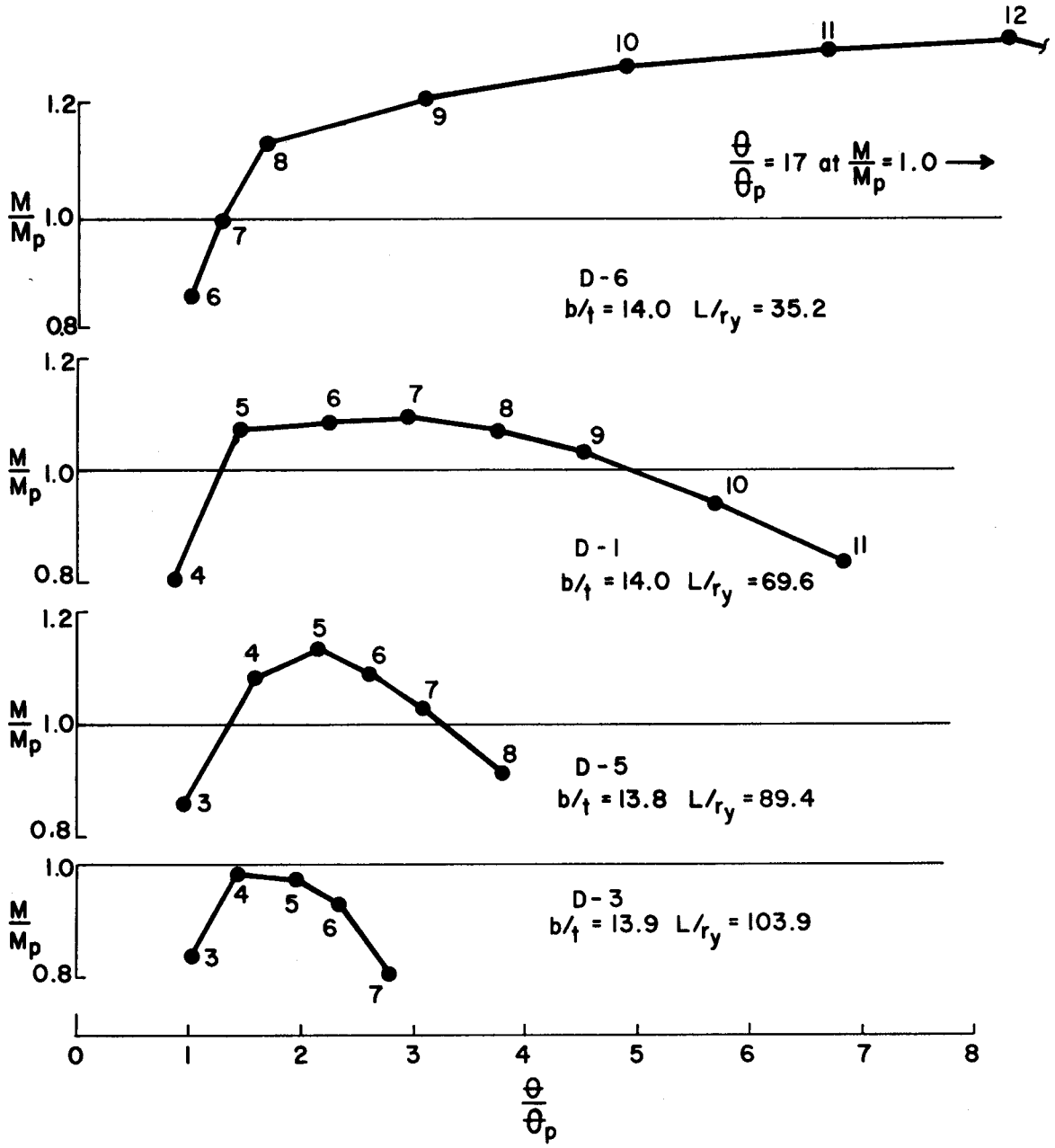

FIGURE 4.10 SERIES D MOMENT-ROTATION RELATIONSHIPS

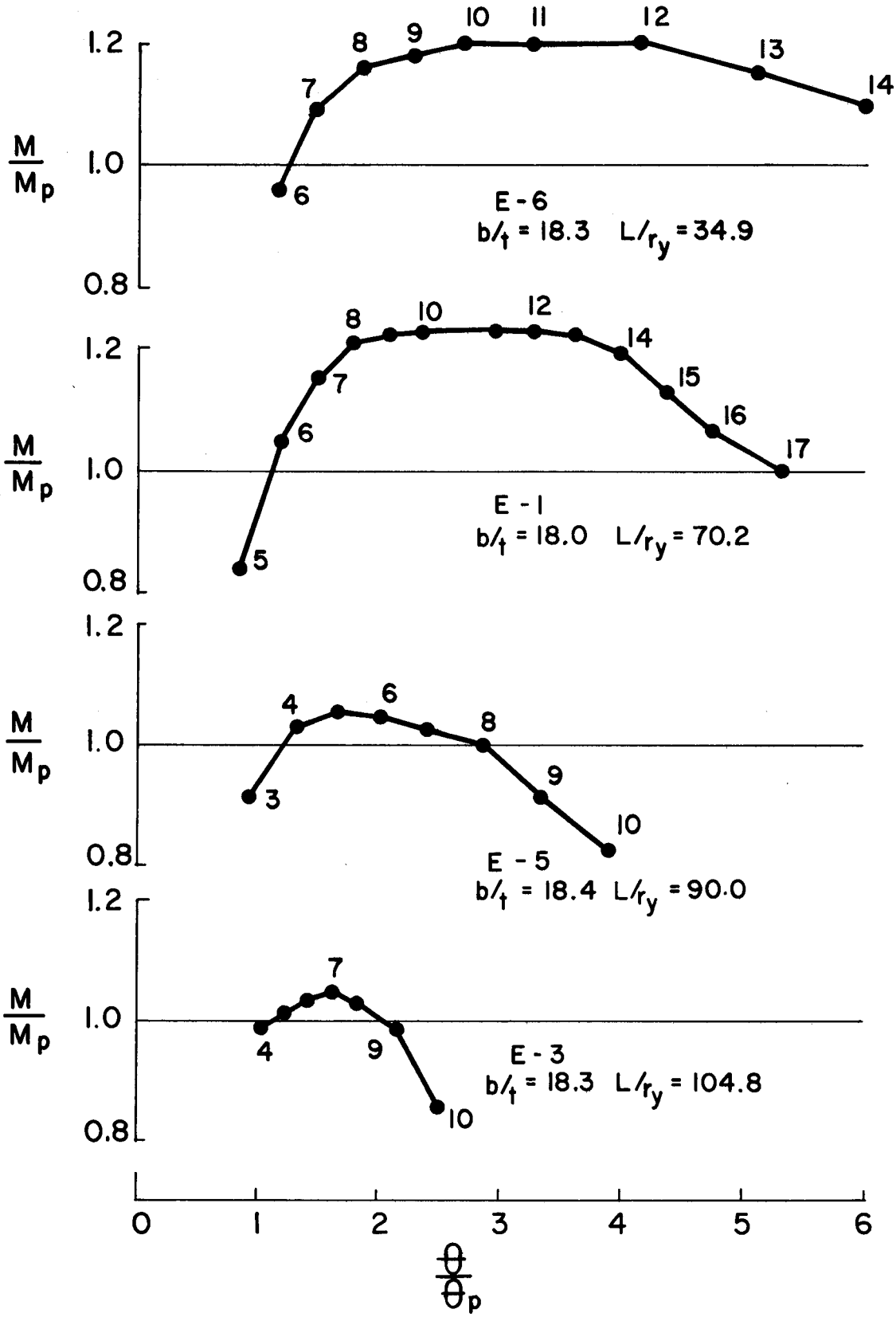

FIGURE 4.11 SERIES E MOMENT-ROTATION RELATIONSHIPS

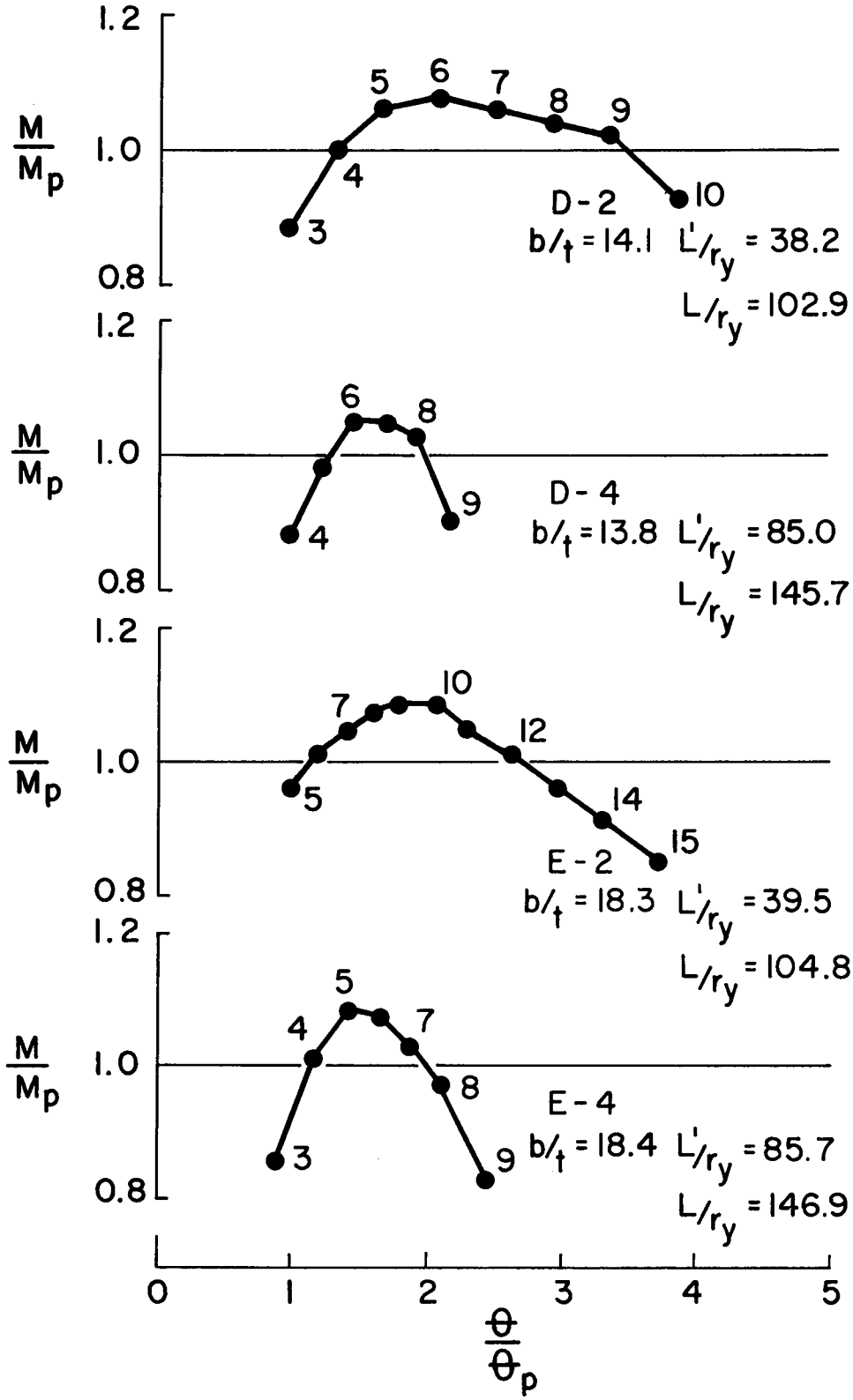

FIGURE 4.12 SERIES D AND E MOMENT-ROTATION RELATIONSHIPS

CHAPTER V

DISCUSSION OF RESULTS

The rotation capacities ($R = \theta/\theta_p - 1$) of the Series D and E beams, obtained from FIGS. 4.10 and 4.11, are summarized in TABLE 5.1 along with the pertinent geometric properties. The flange slenderness ratios, b/t, have been adjusted by the factor $\sqrt{\sigma_y E/44E_{st}}$, where σ_y and E_{st} are the measured yield stress and strain-hardening modulus of the flange. This factor was used to bring the results for members having different yield stress levels and strain-hardening moduli to a common basis. The modulus of elasticity, E, has been taken as 29,600 ksi. The values of the unbraced slenderness ratio, L/r_y, and the slenderness factor, λ, (defined by Eq. 2.1) are also given for the tests. In TABLE 5.1, θ_H, the inelastic hinge capacity of the full span, is taken at the point where M drops below M_p ($\theta_H = R\theta_p$).

TABLE 5.1 presents information (for Series D and E tests) illustrating the influence of the unbraced length, and of necessity the moment gradient, on the rotation capacity. For the beams listed the rotation capacities, R, decreased significantly as the unbraced length increased.

Lay and Galambos have indicated that lateral rather than local buckling will initiate unloading of the member for values of the slenderness factor, λ, above approximately 0.7 [3]. Of the tests listed in TABLE 5.1, the values of λ for the "intermediate" (D-1,D-5,

E-1 and E-5) and "long" (D-3 and E-3) specimens exceed 0.7 . For the short specimens (D-6 and E-6), λ is less than 0.7 , and for this case the inelastic hinge capacities have been related to the optimum yielded length of the compression flange, ℓ_{opt} , given by Eq. (2.2) [3]. This development is valid only for sections having flange slenderness ratios given by Eq. (2.3).

In TABLE 5.2, the predicted inelastic hinge capacities, θ_T , have been listed along with those measured experimentally, θ_u . The predicted capacities, θ_T , have no meaning for the intermediate and long specimens since failure was precipitated by large lateral deformations. The values are included only for the sake of completeness. The actual length of the local buckle, ℓ_u , the yielded length, $\tau_u L$, and the experimentally-determined inelastic hinge rotation, θ_u , were measured at the peak of the M-θ curve. $\tau_u L$ was determined by measuring the average length over which the whitewash had spalled off the compression flange.

For the "short" specimens (D-6 and E-6), in which unloading was triggered by local buckling, the yielded lengths, $\tau_u L$, were smaller than ℓ_{opt} [3]. These were tests in which the yielded lengths were restricted by the high moment gradient. Thus local buckling was initiated at yielded lengths considerably below ℓ_{opt} .

For the "intermediate" specimens (D-1, D-5, E-1 and E-5) the yielded lengths, $\tau_u L$, were greater than ℓ_{opt} . For these tests the local and lateral deformations developed simultaneously. Once the local deformations became severe, the lateral deformations increased rapidly whereas the local deformations increased at a slower rate. This

behavior resulted in large out-of-plane deformations of the unbraced span accompanying unloading of the member.

The yielded lengths, $\tau_u L$, of the "long" specimens (D-3 and E-3) were less than ℓ_{opt} at the peak of the M-θ curve. Unloading was precipitated by large lateral deformations of the unbraced span with no severe local deformations. The large lateral deformations were initiated by lateral imperfections in the member and were accentuated by the slenderness of the unbraced span and the pattern of yielding at the load point. The yielded pattern and lateral deformations of the compression flange of the Series D specimens are shown in FIG. 4.5. As shown in TABLE 5.2, the measured wavelengths of the local buckle, ℓ_u , were approximately one-half of ℓ_{opt} .

FIG. 5.1 summarizes the data contained in TABLE 5.1. This figure plots the rotation capacity, R' , versus the effective slenderness ratio, KL'/r_y . The effective length factors, K , were obtained by considering the lateral bending action of the compression flange of the beam as a restrained column [14]. The values obtained agree with the laterally deflected shape of the compression flange observed during testing. The figure illustrates that for members having small values of KL'/r_y (high moment gradient), where unloading is triggered by local buckling, the flange slenderness ratio, b/t , has a definite effect upon the delivered rotation capacity. This point is illustrated by the results of Tests D-6 and E-6 which had b/t values of 14.0 and 18.3 respectively. For specimens having larger values of KL'/r_y ($KL'/r_y \geq 70$), unloading was due primarily to large lateral deformations, thus b/t has very little effect. This is illustrated by the results of

D-1 and E-1, D-5 and E-5, and D-3 and E-3. In each pair of tests the b/t values were widely separated and yet the delivered rotation capacities were approximately equal. The inelastic hinge capacity decreased as KL'/r_y was increased. The discussion above refers to the tests in which intermediate braces were not used. Tests D-2 and E-2 and D-4 and E-4 will be discussed below.

The inelastic hinge rotations of beams under moment gradient are limited by the extent of yielding at the load point. This yielding in combination with either local deformations or initial lateral imperfections (or both) will cause large out-of-plane deformations of the unbraced span and consequent unloading of the member. No attempt has been made to formulate a theory to predict the complete behavior of the member.

For members having small unbraced slenderness ratios and therefore high moment gradients, the yielded length, $\tau_u L$, will directly affect the correlation between the measured hinge rotations, θ_u, and the predicted rotations, θ_T. Therefore, the predicted values are reduced to compensate for the high moment gradients. The adjusted values of θ_T are $\bar{\theta}_T = \theta_T V_{opt}/V_u$, where V_{opt} is defined as the moment gradient corresponding to $\tau L = \ell_{opt}$ and V_u is the moment gradient on the member at the peak of the M-θ curve [3]. For a yielded length, τL, greater than ℓ_{opt}, the local buckle is not restricted by the extent of yielding and therefore the predicted rotations, θ_T, are constant for all values of $V_u < V_{opt}$.

The ratio V_{opt}/V_u is listed for the tests, in TABLE 5.2, along with the adjusted values of the predicted hinge rotations,

$\bar{\theta}_T$ and the ratios, $\theta_u/\bar{\theta}_T$ and $\theta_H/\bar{\theta}_T$. TABLE 5.3 presents a summary of the results of previous tests [2]. The adjusted hinge rotations, $\bar{\theta}_T$, the rotation capacities, R , and the ratios, V_{opt}/V_u , $\theta_u/\bar{\theta}_T$ and $\theta_H/\bar{\theta}_T$ are listed. The flange slenderness ratio, b/t has been adjusted by the factor $\sqrt{\sigma_y E/44E_{st}}$.

FIG. 5.2 illustrates the behavior of "short" beams in which unloading of the member is a direct result of local buckling within the yielded portion of the compression flange. This figure summarizes the data for all specimens having unbraced slenderness ratios of approximately 35 . The ratio of experimental to predicted rotations, $\theta_u/\bar{\theta}_T$ and $\theta_H/\bar{\theta}_T$, versus $b/t\sqrt{\sigma_y E/44E_{st}}$ are plotted. The tests include specimens in which the length of the local buckle was restricted by the high moment gradient $(V_{opt}/V_u < 1.0)$ and specimens in which V_u was less than V_{opt} , so that the buckled wavelength was not restricted by the extent of yielding.

From the results of a previous investigation it was postulated that the inelastic hinge rotation of beams having low moment gradients are not necessarily limited by the attainment of a yielded length equal to the optimum wavelength of the local buckle [2].

However, the present experimental results do not confirm this trend. If the ratio $\theta_u/\bar{\theta}_T$ is plotted versus the flange slenderness ratio $b/t\sqrt{\sigma_y/44}$; the Series A tests (beams under low moment gradients but having a large E_{st} value) plotted well above the others [2]. If, however, the flange slenderness ratios are adjusted by the factor $\sqrt{\sigma_y E/44E_{st}}$; the results of all tests plot as a narrow band. The plot in FIG. 5.2 illustrates that for "short" specimens $(L/r_y = 35)$ and

therefore high moment gradients, the delivered rotation capacities are dependent upon the flange slenderness ratio, b/t , and the material properties, namely; the yield stress and the strain-hardening modulus. The specimens with intermediate braces, having an effective slenderness ratio (KL'/r_y) of approximately 35 , were not included in FIG. 5.2 because unloading of these members does not appear to be dependent on the b/t ratio.

The results of Lehigh tests, performed on A441 steel beams under moment gradient have not been included in FIG. 5.2 as the values of the strain-hardening moduli for these specimens were unavailable [5].

The data for the specimens having intermediate braces are summarized in TABLE 5.4. The inelastic hinge capacity, R , the experimentally -determined hinge rotation, θ_H , and the half-span slenderness ratio, L/r_y , have been listed for the tests. The flange slenderness ratio, b/t , has been adjusted by the factor $\sqrt{\sigma_y E/44E_{st}}$. Both the unbraced slenderness ratio, L'/r_y , and λ have been adjusted to their effective values. In each of the tests listed in TABLE 5.4, having approximately the same b/t and KL'/r_y values (e.g. D-6 and D-2), the experimental inelastic rotations, θ_H , of the beams under lower moment gradient were approximately one-half those of the specimens under higher moment gradient. The delivered rotation capacities, for the beams having intermediate braces as shown in FIG. 5.1, were much below those expected. The results plotted on FIG. 5.1 indicate that since R was independent of b/t , unloading was essentially the result of large lateral deformations. In fact, the test specimens having intermediate braces delivered rotation capacities only slightly greater

than those delivered by comparable specimens without intermediate lateral braces. This would indicate that the large yielded lengths (due to the low moment gradients on the members) have a dominant influence on the member behavior [15].

In TABLE 5.5, the values of $\tau_u L$, ℓ_{opt} , ℓ_u , θ_u and θ_T are listed. Along with the adjusted hinge rotations, $\bar{\theta}_T$ the ratios V_{opt}/V_u , $\theta_u/\bar{\theta}_T$ and $\theta_H/\bar{\theta}_T$ are also given. In TABLE 5.5, the yielded lengths, $\tau_u L$, of the specimens under lower moment gradient (having the intermediate braces) were greater than ℓ_{opt} . At the onset of local deformations for specimens D-2 and E-2 the yielded lengths were of sufficient magnitude to precipitate large lateral deformations of the unbraced span and consequent unloading of the member. For specimens D-4 and E-4 the initial imperfections coupled with yielding lead to large lateral deformations of the unbraced span before the occurrance of local deformations. The yielded pattern and lateral deformations of the compression flange of beam E-4 are shown in FIG. 5.3.

Test	$\frac{b}{t}\sqrt{\frac{\sigma_y E}{44E_{st}}}$	$\frac{L}{r_y}$	θ_H	$R=\frac{\theta_H}{\theta_p}-1$	λ
D-6	120	35.2	0.136	15.9	0.43
D-1	114	69.6	0.064	3.9	0.83
D-5	120	89.4	0.047	2.2	1.06
D-3	118	103.9	0.0	0.0	1.27
E-6	157	34.9	0.083	7.2	0.43
E-1	153	70.2	0.098	4.3	0.86
E-5	152	90.0	0.054	1.9	1.08
E-3	149	104.8	0.033	1.0	1.24

TABLE 5.1 SERIES D AND E - TOTAL ROTATIONS

Test	$\tau_u L$	ℓ_{opt}	ℓ_u	θ_u	θ_T	$\frac{V_{opt}}{V_u}$	$\bar{\theta}_T=\theta_T\frac{V_{opt}}{V_u}$	$\frac{\theta_u}{\bar{\theta}_T}$	$\frac{\theta_H}{\bar{\theta}_T}$
D-6	4.5	5.03	3.5	0.0624	0.0484	0.745	0.0360	1.73	3.78
D-1	6.5	5.03	3.5	0.0318	0.0448	1.89	0.0448	0.71	1.43
D-5	7.5	5.03	2.5	0.0242	0.0413	2.40	0.0413	0.59	1.14
D-3	4.0	5.03	-	0.0	0.0421	2.96	0.0421	0.0	0.0
E-6	4.0	6.12	3.5	0.0360	0.0589	0.940	0.0553	0.65	1.50
E-1	6.0	6.12	3.0	0.0372	0.0512	1.78	0.0512	0.73	1.92
E-5	8.5	6.12	3.0	0.0194	0.0619	2.91	0.0619	0.31	0.87
E-3	5.5	6.12	3.5	0.0198	0.0473	3.44	0.0473	0.42	0.70

TABLE 5.2 SERIES D AND E - YIELDED LENGTHS, PEAK AND ADJUSTED ROTATIONS

Test	$\frac{b}{t}\sqrt{\frac{\sigma_y E}{44E_{st}}}$	R	$\frac{V_{opt}}{V_u}$	$\bar{\theta}_T$	$\frac{\theta_u}{\bar{\theta}_T}$	$\frac{\theta_H}{\bar{\theta}_T}$
A-2	96	13.6	1.14	0.0603	2.02	4.51
A-1	111	11.8	1.26	0.0674	1.69	3.86
B-2	125	10.4	0.595	0.0455	1.07	2.64
B-3	145	6.7	0.633	0.0545	0.95	1.69
B-4	159	3.4	0.741	0.0682	0.44	0.76
B-5	163	3.2	0.757	0.0711	0.42	0.67
B-1	173	2.9	0.746	0.0733	0.38	0.57
C-2	118	13.7	0.606	0.0309	1.56	3.63
C-3	137	8.0	0.710	0.0405	0.73	1.93
C-5	144	6.5	0.747	0.0442	0.72	1.54
C-4	150	4.2	0.764	0.0464	0.47	0.97
C-1	163	4.2	0.770	0.0500	0.47	0.98

TABLE 5.3 SERIES A, B AND C - TEST RESULTS

Test	$\frac{b}{t}\sqrt{\frac{\sigma_y E}{44E_{st}}}$	$\frac{L}{r_y}$	$\frac{KL'}{r_y}$	θ_H	$R=\frac{\theta_H}{\theta_p}-1$	λ
D-6	120	35.2	35.2	0.136	15.9	0.43
D-2	116	102.9	33.7	0.061	2.5	0.40
E-6	157	34.9	34.9	0.083	7.2	0.43
E-2	149	104.8	34.8	0.055	1.7	0.41
D-1	114	69.6	69.6	0.064	3.9	0.83
D-4	120	145.7	69.4	0.033	1.0	0.82
E-1	153	70.2	70.2	0.098	4.3	0.86
E-4	150	146.9	70.0	0.046	1.0	0.83

TABLE 5.4 SERIES D AND E - TOTAL ROTATIONS

Test	$\tau_u L$	ℓ_{opt}	ℓ_u	θ_u	θ_T	$\frac{V_{opt}}{V_u}$	$\bar{\theta}_T=\theta_T\frac{V_{opt}}{V_u}$	$\frac{\theta_u}{\bar{\theta}_T}$	$\frac{\theta_H}{\bar{\theta}_T}$
D-6	4.5	5.03	3.5	0.0624	0.0484	0.745	0.0360	1.73	3.78
D-2	7.0	5.03	3.0	0.0264	0.0508	2.84	0.0508	0.52	1.21
E-6	4.0	6.12	3.5	0.0360	0.0589	0.940	0.0553	0.65	1.50
E-2	10.0	6.12	3.5	0.0300	0.0545	3.32	0.0545	0.55	1.02
D-1	6.5	5.03	3.5	0.0318	0.0448	1.89	0.0448	0.71	1.43
D-4	7.5	5.03	3.0	0.0156	0.0413	4.22	0.0413	0.38	0.80
E-1	6.0	6.12	3.0	0.0372	0.0512	1.78	0.0512	0.73	1.92
E-4	9.0	6.12	-	0.0190	0.0473	4.64	0.0473	0.40	0.98

TABLE 5.5 SERIES D AND E - YIELDED LENGTHS, PEAK AND ADJUSTED ROTATIONS

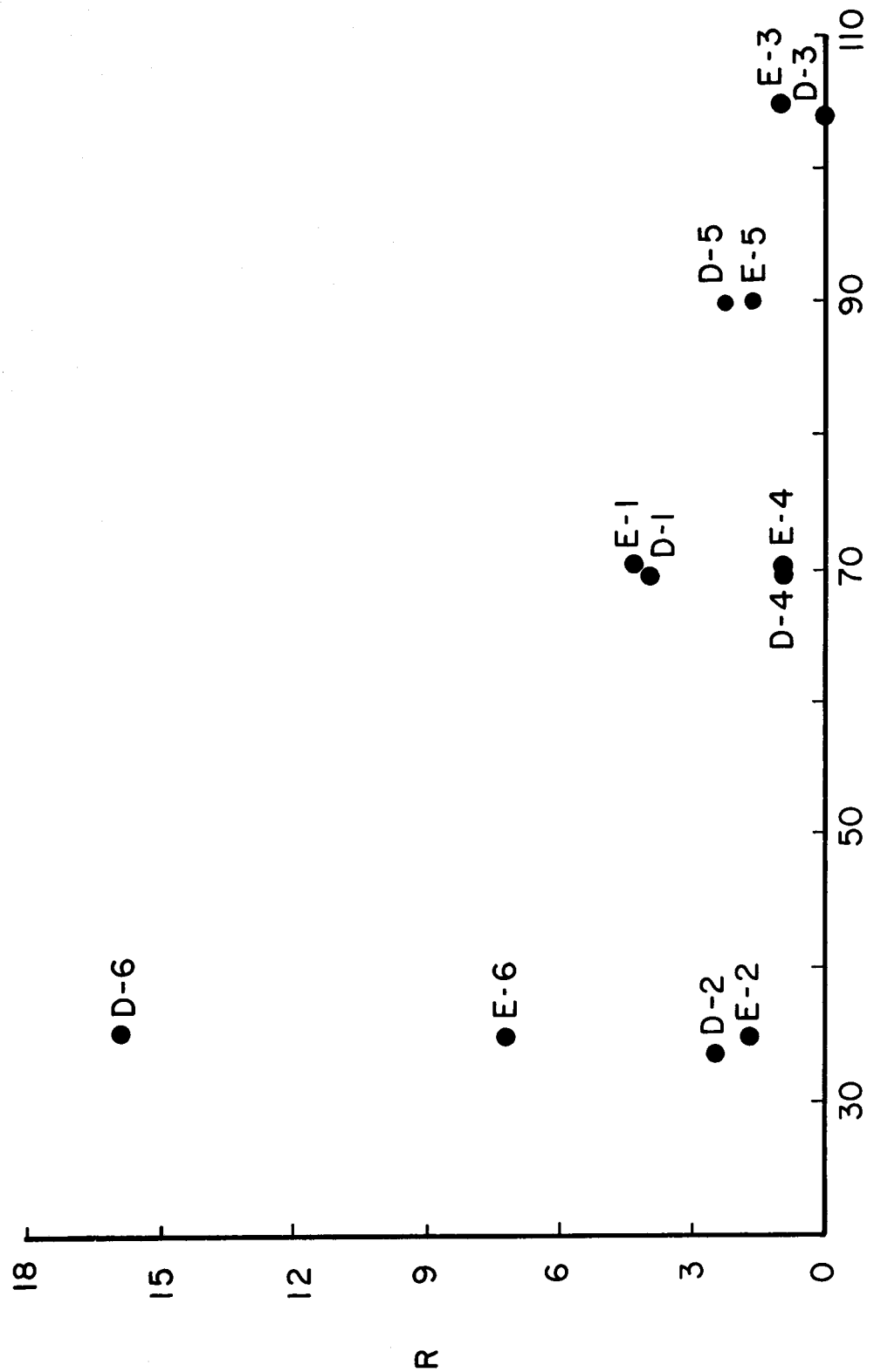

FIGURE 5.1 ROTATION CAPACITIES

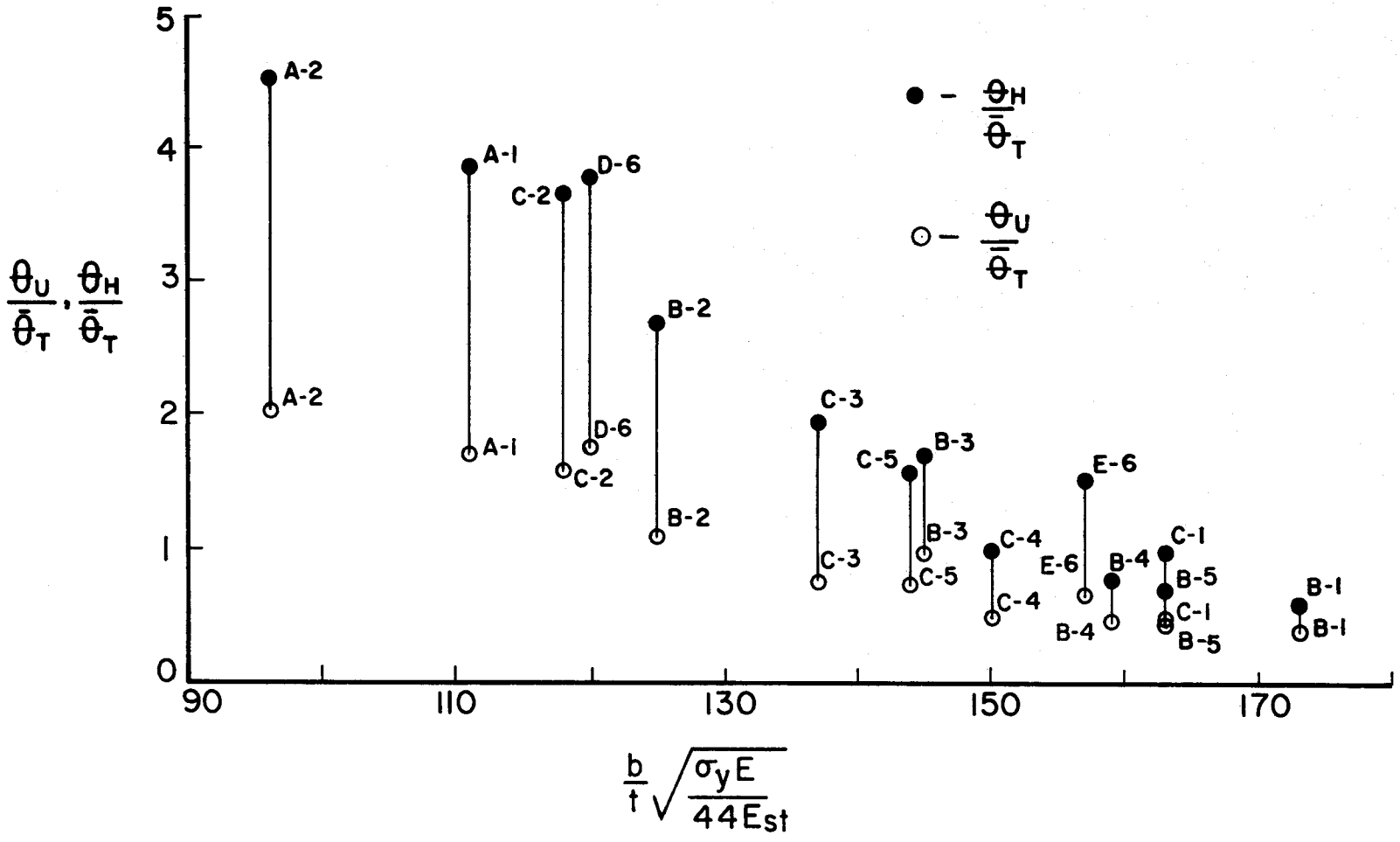

FIGURE 5.2 PEAK AND TOTAL ROTATIONS - EXPERIMENTAL/THEORETICAL

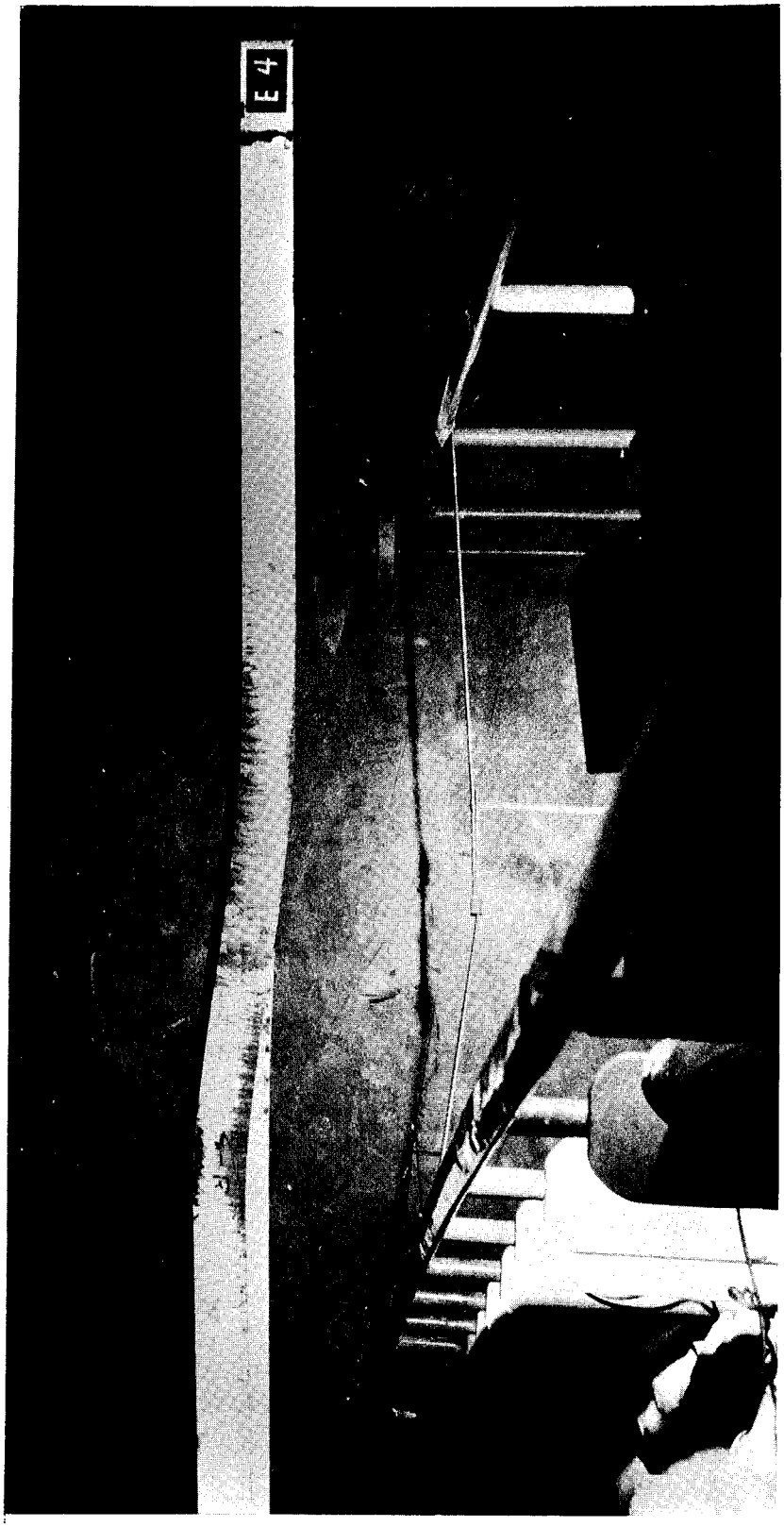

FIGURE 5.3 LATERAL DEFORMATION OF BEAM E-4

CHAPTER VI

CONCLUSIONS AND RECOMMENDATIONS

The analysis of a three-span continuous beam has been used to estimate the maximum rotation capacities required for the formation of a mechanism [16]. For practical cases, the magnitude of the maximum required hinge rotation is $\theta_R = 1.66\ \varepsilon_y f L/d$, where f is the shape factor of the beam cross-section [2]. This hinge requirement is based on simple plastic theory. More exact analysis has shown that the simple plastic theory overestimates the true requirements [17].

The hinge rotation requirement (θ_R) for a continuous beam can be related to the delivered hinge capacity of a particular test specimen by determining the continuous beam span which is equivalent to that of the test specimen. By comparing the moment diagram of the continuous beam and the test beam, it was found that the equivalent span of the continuous beam is approximately $4L/5$ [2]. The required hinge rotation is then calculated for the equivalent continuous beam.

In TABLE 6.1, the equivalent span to depth ratio, $4L/5d$, and the required hinge rotation, θ_R, are listed for the tests, along with the adjusted values of the hinge rotation, $\bar{\theta}_H = \theta_H\ V_u/V_{opt}$. The factor V_u/V_{opt} (if ≥ 1) is applied to account for the restriction of the yielded lengths due to the high moment gradients.

For the "short" specimens (D-6 and E-6), as well as for tests reported in a previous report, $\bar{\theta}_H$ was greater than θ_R [2]. This implies

that the hinge rotation requirements for "short" beams can easily be met, even by the most slender-flanged sections.

The very long members, however, require the largest hinge rotations. Because of the limitations on allowable working load deflections, the L/d ratio is assumed to be less than 40 for wide-flange beams having a yield stress of 44 ksi. Therefore the maximum required hinge capacity (assuming $L/d = 40$, $\sigma_y = 44$ ksi and $f = 1.15$) has been calculated as $\theta_R = 0.113$ radians [2].

The values of $\bar{\theta}_H$, for the "intermediate" specimens (D-1, D-5, E-1 and E-5), having equivalent span to depth ratios approximately equal to one-quarter of the maximum allowable, were also greater than that required by the continuous beam analysis. However for the "long" specimens (D-3 and E-3), with L/d ratios approximately one-half the allowable, the adjusted hinge rotations do not meet those required.

The use of intermediate braces had a beneficial effect by increasing the inelastic hinge rotations, however, for the longest specimens tested (D-4 and E-4), with L/r_y approximately 147, KL'/r_y approximately 70 and $4L/5d$ approximately one-half of the maximum allowable, the required hinge rotation (θ_R) was still greater than the delivered hinge rotation $(\bar{\theta}_H)$.

These trends would indicate that the required inelastic rotations cannot be delivered by long beams. However, this does not seem reasonable. It is recommended that a further study be carried out using a more exact analysis to determine the required hinge rotations. This study would use the actual curvature distribution over the beam length.

In company with the more accurate prediction of θ_R , a theory would have to be formulated to account for the inelastic behavior of longer specimens. Thus unloading triggered by local buckling and unloading which is primarily a result of large out-of-plane deformations of the unbraced span would have to be considered. No attempt has been made to formulate a theory incorporating these factors.

The Canadian Standards Association has defined a compact section as one in which the projecting elements of the compression flange shall have a width-to-thickness ratio less than $54/\sqrt{F_y}$ [9].

For beams tested under moment gradient the yielded length extends along the length of the member from the point of maximum moment. When the yield point stress is attained, a strain jump occurs from the yield strain, ε_y , to the strain at the onset of strain-hardening, ε_{st} . Thus when local buckling occurs, the material in the yielded portion of the compression flange has been strain-hardened. This would imply for most cases (and in fact for all cases tested) that the moment has exceeded M_p . Therefore the allowable stress design rules for the flange slenderness ratio (b/t) of a compact section can be based on the results of short wide-flange beams tested under moment gradient.

As previously discussed, the flange slenderness ratio, b/t , had relatively little effect on specimens with $L/r_y \geq 70$. However, for the "short" specimens (in which unloading was triggered by local deformations) the delivered rotation capacity, R , was directly influenced by b/t . If b/t is calculated from the present C.S.A. Code rule $(b/2t \leq 54/\sqrt{F_y})$ using a yield stress, F_y , of 44 ksi

a b/t value of 16.3 is obtained. Using the smallest value obtained for the strain-hardening modulus (E_{st} = 363 ksi) the ratio $\sqrt{E/E_{st}}$ is 9.04 . The smallest observed value of E_{st} was used in order to predict the most conservative value (in this case the smallest value) of the rotation capacity. Thus any increase in E_{st} (above that used in this development) would result in an increased hinge rotation. The factor $b/t\sqrt{F_y E/44E_{st}}$ has a value of 147 which corresponds, in FIG. 6.1, to a delivered rotation capacity of approximately 6 . This large value of R indicates that for working stress design the current code limitations on b/t could be relaxed.

To obtain a value of R approximately equal to 2.5 would be quite satisfactory and still conservative. The factor $b/t\sqrt{F_y E/44E_{st}}$, from FIG. 6.1, would then be approximately equal to 174 and would result in a b/2t value of 9.65 (or b/t = 19.3). Substituting this value into the form of the present code, $b/t = C/\sqrt{F_y}$, where F_y = 44 ksi; the value of the constant, C , would be approximately equal to 64 . Therefore it is proposed that in working stress design, for a section to qualify as compact, the projecting elements of the compression flange shall have a width-to-thickness ratio not exceeding $64/\sqrt{F_y}$.

A limiting b/t value for plastic design rules cannot be recommended until a closer estimate of the required rotation capacity for the plastic design of continuous beams has been developed.

Test	$\frac{4}{5}\frac{L}{d}$	θ_R	$\bar{\theta}_H$
D-6	3.52	0.0100	0.183
D-1	7.02	0.0186	0.064
D-5	9.01	0.0235	0.047
D-3	10.50	0.0294	0.0
D-2	10.36	0.0278	0.061
D-4	14.74	0.0385	0.033
E-6	4.92	0.0140	0.088
E-1	9.84	0.0275	0.098
E-5	12.69	0.0341	0.054
E-3	14.78	0.0386	0.033
E-2	14.78	0.0392	0.055
E-4	20.70	0.0540	0.046

TABLE 6.1 SERIES D AND E - REQUIRED AND ADJUSTED ROTATIONS

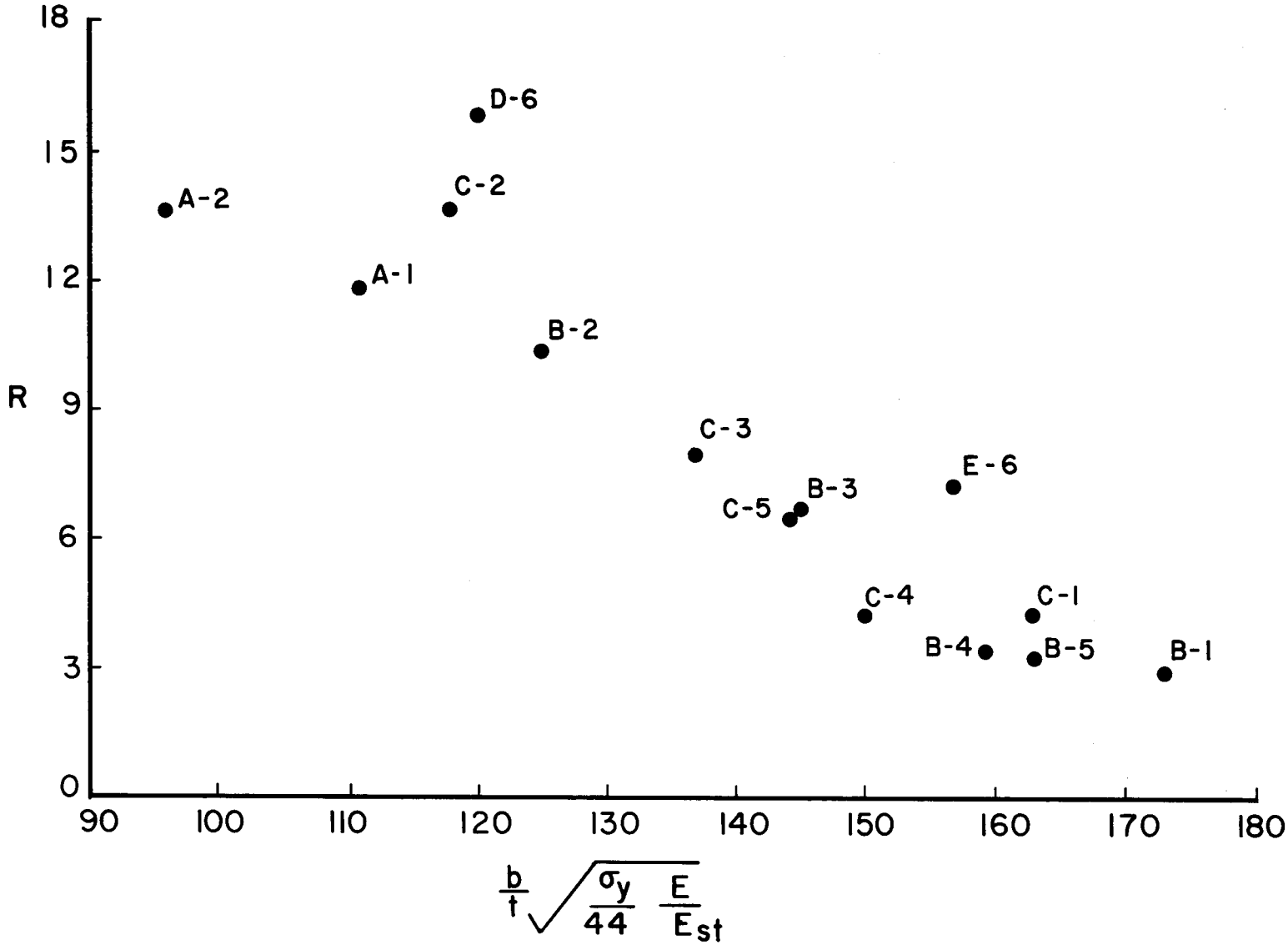

FIGURE 6.1 ROTATION CAPACITIES OF SHORT BEAMS

CHAPTER VII

SUMMARY

This investigation was undertaken to define the effect of moment gradient on the rotation capacity of steel wide-flange beams and to separate the influence of moment gradient from that of the unbraced slenderness ratio. In addition, an attempt was made to differentiate between unloading triggered by local buckling and unloading which resulted primarily from large lateral-torsional deformations.

The experimental program reported herein consisted of two series of six tests on rolled wide-flange steel beams, having a range of L/r_y values from approximately 35 to 147 . The two test series, D and E, had flange slenderness ratios (b/t) of approximately 14.0 and 18.3 , respectively. The specimens were simply supported and subjected to a concentrated load at midspan. Lateral bracing was provided at the load and reaction points, and for some specimens at two intermediate locations. All tests were continued well into the unloading range.

A wide range of rotation capacities was observed for the beams tested. The members having large unbraced lengths delivered smaller rotation capacities than did the shorter members. For "short" specimens unloading was triggered by local buckling, whereas

for the longer specimens, unloading was due primarily to the large lateral deformations. These deformations were initiated by the initial imperfections of the unbraced span and accentuated by the yielded pattern of the compression flange at the load point.

The test results indicated that for members having small values of L/r_y (high moment gradient), where unloading was triggered by local deformations, the flange slenderness ratio, b/t, had a definite effect upon the delivered rotation capacity (R). For specimens of larger unbraced length ($L/r_y \geq 70$), in which unloading was due primarily to large lateral deformations, b/t had very little effect. For tests on specimens having intermediate lateral braces and low moment gradients unloading was also due to lateral deformations. These specimens delivered rotation capacities much below those expected and furthermore R was approximately constant for tests with varying b/t ratios. This indicates that b/t had little effect on the rotation capacities of these members.

Since only the hinge capacities of short beams were governed by the flange slenderness ratio, a specific design recommendation was made regarding the limiting b/t value for compact sections. This recommendation stated that for a section to qualify as a compact section in working stress design only; the maximum width-to-thickness ratio for projecting elements of the compression flange could be changed from $54/\sqrt{F_y}$ to $64/\sqrt{F_y}$. A limiting b/t value was not recommended for members designed by the plastic method because the rotation capacities required for continuous beams have not yet been determined.

The hinge capacities delivered by the test specimens were

compared to the maximum requirement, based on simple plastic theory, for continuous beams of practical dimension. For the shorter specimens the inelastic rotation requirements were easily met, whereas for the longer specimens, the delivered hinge rotations were less than those required. Therefore, a theoretical analysis was proposed to calculate a more exact value of the required hinge rotation. It is expected that the results of this analysis, in conjunction with the presently available test results, would provide sufficient basis upon which to make specific design recommendations for the plastic design of long beams under moment gradient.

NOMENCLATURE

A_f	Flange area
A_w	Web area
b	Flange width
d	Depth of section
E	Modulus of elasticity
E_{st}	Strain-hardening modulus
f	Shape factor
F_y	Yield stress
h	Ratio of elastic to strain-hardening modulus
I	Moment of inertia
I_{yy}	Moment of inertia about weak axis
K	Effective length factor
L	Span length
L'	Length from load point to intermediate lateral brace
ℓ_{opt}	Theoretical optimum wavelength of local buckle
ℓ_u	Measured wavelength of local buckle at maximum moment
M	Moment
M_o	Maximum moment
M_p	Plastic moment
P	Load
R	Rotation capacity

r_y	Weak axis radius of gyration
S	Adjacent span spring constant
s	Ratio of strain-hardening strain to yield strain
t	Flange thickness
u	Lateral displacement of compression flange
V_{opt}	Shear force corresponding to a yielded flange length of ℓ_{opt}
V_u	Maximum attained shear force
w	Thickness of web
ε	Strain
ε_{st}	Strain at onset of strain-hardening
ε_y	Yield strain
θ	Rotation
θ_H	Inelastic hinge rotation (hinge capacity)
$\bar{\theta}_H$	Maximum hinge capacity adjusted for effect of high moment gradient
θ_p	Rotation corresponding to attainment of M_p
θ_R	Required hinge capacity
θ_T	Theoretical delivered hinge capacity
$\bar{\theta}_T$	Theoretical delivered hinge capacity adjusted for effect of high moment gradient
θ_u	Delivered inelastic hinge rotation at maximum moment
λ	Slenderness factor
σ	Stress
σ_u	Ultimate stress
σ_y	Yield stress
τ	Proportion of flange length yielded
τ_u	Proportion of flange length yielded at maximum moment

ϕ_p Curvature corresponding to M_p assuming ideally elastic material

υ Vertical deflection at midspan

δ Out-of-plane displacement of the compression flange

LIST OF REFERENCES

1. Errera, S. J. - "Structural Steel Design", Chapter 2, Materials, The Ronald Press Company, New York, 1964

2. Lukey, A. F. and Adams, P. F. - "Rotation Capacity of Wide-Flange Beams Under Moment Gradient", Department of Civil Engineering, Edmonton, Alberta, Canada, May 1967

3. Lay, M. G. and Galambos, T. V. - "Inelastic Beams Under Moment Gradient", Proc. ASCE, Vol. 93, ST1, February 1967

4. White, M. W. - "The Lateral-Torsional Buckling of Yielded Structural Steel Members", Ph.D. Dissertation, Lehigh University, Bethlehem, Pa., 1956

5. Adams, P. F., Lay, M. G. and Galambos, T. V. - "Experiments on High Strength Steel Members", Welding Research Council Bulletin No. 110, November 1965

6. Sawyer, H. A. Jr. - "Post-Elastic Behavior of Wide-Flange Steel Beams", Proc. ASCE, Vol. 87, ST8, December 1961

7. Lay, M. G. - "Flange Local Buckling in Wide-Flange Shapes", Proc. ASCE, Vol. 91, ST6, December 1965

8. Haaijer, G. and Thurlimann, B. - "Local Buckling of Wide-Flange Shapes", Lehigh University, Fritz Laboratory Report No. 205E.5, December 1954

9. CSA - "Steel Structures for Buildings", Canadian Standards Association Standard S-16, 1965

10. AISC - "Specification for the Design, Fabrication and Erection of Structural Steel for Buildings", American Institute of Steel Construction, 1961

11. Massey, C. and Pitman, F. S. - "Inelastic Lateral Stability Under a Moment Gradient", Proc. ASCE, Vol. 92, EM2, April 1966

12. CSA - "General Purpose Structural Steel", Canadian Standards Association Standard G40.12, 1964

13. Adams, P. F. and Galambos, T. V. - "Material Considerations in Plastic Design", Lehigh University, Fritz Laboratory Report No. 297.23, November 1966

14. Bleich, F. - "Buckling Strength of Metal Structures", McGraw-Hill Book Company, Inc., New York, 1952

15. Lay, M. G. and Galambos, T. V. - "Inelastic Steel Beams Under Uniform Moment", Proc. ASCE, Vol. 91, ST6, December 1965

16. Kerfoot, R. P. - "Rotation Capacity of Beams", Lehigh University, Fritz Laboratory Report No. 297.14, March 1965

17. Adams, P. F. - "Plastic Design in High Strength Steel", Lehigh University, Fritz Laboratory Report No. 297.19, May 1966

ACKNOWLEDGEMENTS

This study is part of a continuing investigation "Local Buckling of High Strength Steel Members" currently in progress at the Department of Civil Engineering, University of Alberta. The project is sponsored financially by the Canadian Steel Industries Construction Council, with technical assistance from the Canadian Institute of Steel Construction.

The assistance and interest of Mr. A. J. M. Aikman, Alberta Regional Engineer, C.I.S.C.; Mr. W. R. Sanderson, Chairman, Engineering and Research Sub-Committee of the Alberta Regional Committee, C.I.S.C.; and Mr. H. A. Krentz, Assistant Chief Engineer, C.I.S.C. is particularly acknowledged. The scholarship provided by the Alberta Regional Committee, C.I.S.C., received by R. J. Smith, is also acknowledged.

The assistance of Mr. H. Panse and members of the laboratory staff in the performance of the testing program, and Mrs. E. Smith, and Miss E. Elford, who typed the report, is also acknowledged.